iScience

CellPress

Article

Fate Distribution and Regulatory Role of Human Mesenchymal Stromal Cells in Engineered Hematopoietic Bone Organs

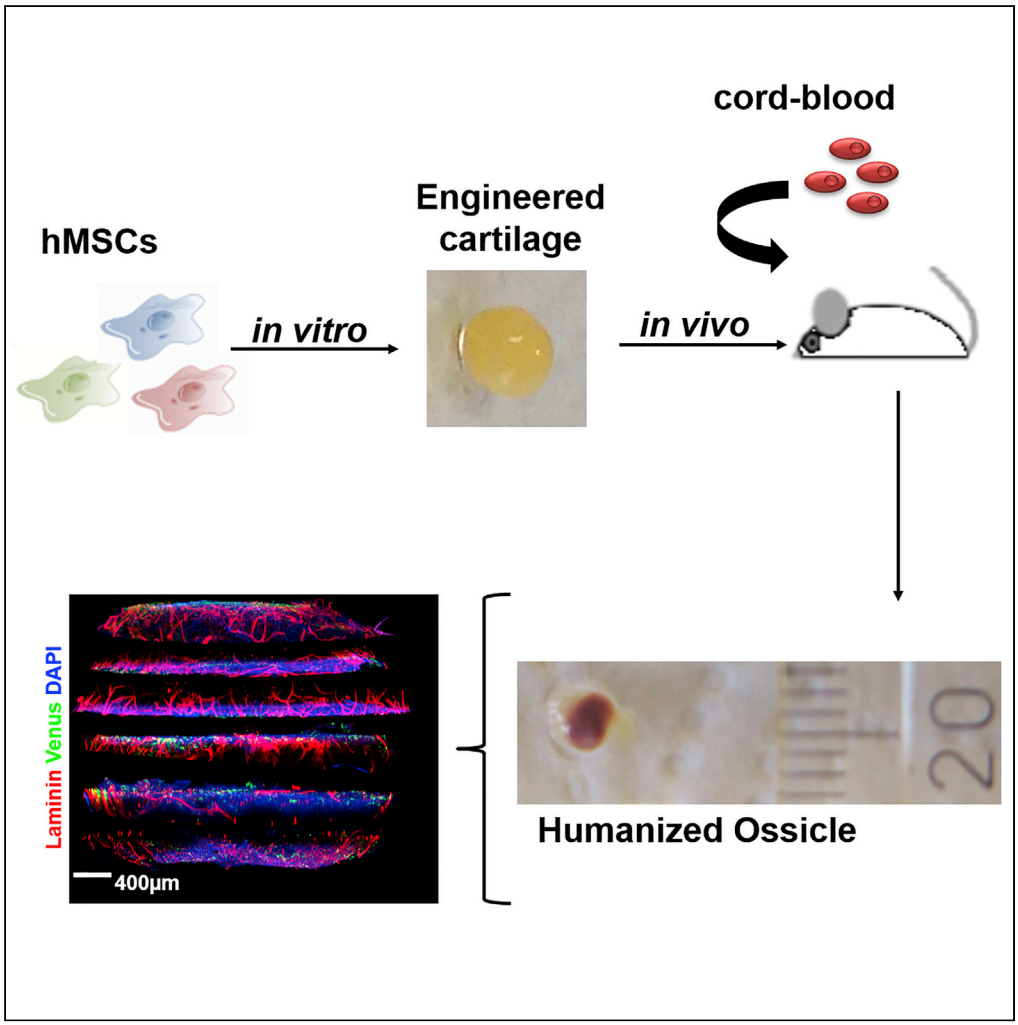

Paul E. Bourgine, Kristin Fritsch, Sebastien Pigeot, ..., Markus G. Manz, Ivan Martin, Timm Schroeder

markus.manz@usz.ch (M.G.M.)
ivan.martin@usb.ch (I.M.)
timm.schroeder@bsse.ethz.ch (T.S.)

HIGHLIGHTS

Mesenchymal cells can generate human bone organs with tailored molecular signature

Mesenchymal cells reconstitute a human niche environment capable of regulating HSPCs

Bourgine et al., iScience *19*, 504–513
September 27, 2019
https://doi.org/10.1016/j.isci.2019.08.006

iScience

CellPress

Article

Fate Distribution and Regulatory Role of Human Mesenchymal Stromal Cells in Engineered Hematopoietic Bone Organs

Paul E. Bourgine,[1,2,5,6] Kristin Fritsch,[3] Sebastien Pigeot,[2] Hitoshi Takizawa,[4] Leo Kunz,[1] Konstantinos D. Kokkaliaris,[1] Daniel L. Coutu,[1] Markus G. Manz,[2,*] Ivan Martin,[2,*] and Timm Schroeder[1,7,*]

SUMMARY

The generation of humanized ectopic ossicles (hOss) in mice has been proposed as an advanced translational and fundamental model to study the human hematopoietic system. The approach relies on the presence of human bone marrow-derived mesenchymal stromal cells (hMSCs) supporting the engraftment of transplanted human hematopoietic stem and progenitor cells (HSPCs). However, the functional distribution of hMSCs within the humanized microenvironment remains to be investigated. Here, we combined genetic tools and quantitative confocal microscopy to engineer and subsequently analyze hMSCs' fate and distribution in hOss. Implanted hMSCs reconstituted a humanized environment including osteocytes, osteoblasts, adipocytes, and stromal cells associated with vessels. By imaging full hOss, we identified rare physical interactions between hMSCs and human CD45+/CD34+/CD90+ cells, supporting a functional contact-triggered regulatory role of hMSCs. Our study highlights the importance of compiling quantitative information from humanized organs, to decode the interactions between the hematopoietic and the stromal compartments.

INTRODUCTION

The lifelong production of all human blood cell lineages is ensured by hematopoietic stem cells (HSCs) (Méndez-Ferrer et al., 2010; Morrison and Scadden, 2014). In adults, HSCs' functions are maintained and tightly regulated in the specialized bone marrow (BM) microenvironment, referred to as the BM niche (Méndez-Ferrer et al., 2010; Morrison and Scadden, 2014). This environment is defined by unique physical properties (Engler et al., 2006; Guilak et al., 2009; Keung et al., 2010) and includes differentiated cells, extracellular matrix, and signaling factors (Rieger et al., 2009; Zhang and Lodish, 2008) essential for cell differentiation, survival (Knapp et al., 2016), and self-renewal (Kunisaki and Frenette, 2012; Méndez-Ferrer et al., 2010). However, the precise cellular and molecular composition of the human hematopoietic niche remains elusive (Bourgine et al., 2018; van Pel et al., 2015). Our understanding of human hematopoiesis largely relies on the analogy made with the mouse system (Schepers et al., 2015). In reality, despite commonly inherited genetic traits, HSC basic biology differs across species and the corresponding interactions with their niches are not fully conserved (Doulatov et al., 2012; van Pel et al., 2015). In consequence, information derived from murine studies does not systematically correlate with the human system, raising concerns about their direct relevance toward therapeutic developments (Doulatov et al., 2012).

Advanced xenotransplantation models offer robust engraftment and development of human hematopoiesis in mouse bones (Rongvaux et al., 2014). This has significantly contributed to the progressive understanding of human HSC functions in healthy and pathological setups (Antonelli et al., 2016; Reinisch et al., 2016). However, such humanized mouse models are incompatible with the organizational and functional study of the HSC niche, because the BM microenvironment remains entirely murine.

As an alternative, the possibility to engineer ectopic humanized ossicles (hOss) using human BM-derived mesenchymal stromal cells (hMSCs) is receiving increasing attention (Bourgine et al., 2014; Reinisch et al., 2016; Scotti et al., 2013), with demonstration of robust human blood engraftment in both healthy and malignant scenarios (Abarrategi et al., 2017; Martine et al., 2017; Reinisch et al., 2016). Although this is attributed to the presence of hMSCs, their contribution in the functional organization of the niche remains to be investigated.

[1]Department of Biosystems Science and Engineering (D-BSSE), ETH Zurich, Mattenstrasse 26, 4058 Basel, Switzerland

[2]Tissue Engineering, Department of Biomedicine, University of Basel and University Hospital Basel, 4056 Basel, Switzerland

[3]Department of Hematology, University Hospital Zurich and University of Zurich, 8091 Zurich, Switzerland

[4]International Research Center for Medical Sciences, Kumamoto University, Kumamoto 860-0811, Japan

[5]Department of Clinical Sciences, Lund Stem Cell Center, Lund University, BMC B11, 221 84 Lund, Sweden

[6]Wallenberg Centre for Molecular Medicine, Lund University, Lund, Sweden

[7]Lead Contact

*Correspondence: markus.manz@usz.ch (M.G.M.), ivan.martin@usb.ch (I.M.), timm.schroeder@bsse.ethz.ch (T.S.)

https://doi.org/10.1016/j.isci.2019.08.006

Here, we propose the genetic engineering of hMSCs together with the use of a recently developed deep multicolor imaging confocal analysis (Coutu et al., 2017) to achieve a first quantitative assessment of the distribution and role of hMSCs in hOss. We previously reported a developmental approach to bone organ formation, by *in vitro* chondrogenic priming of hMSCs (Bourgine et al., 2014; Scotti et al., 2013). Following hypertrophic cartilage (hyC) formation, the generated tissues remodel into hOss upon subcutaneous implantation in humanized mice (Fritsch et al., 2018) by recapitulating the endochondral ossification process (Kronenberg and Kronenberg, 2003). We target the further exploitation of this approach to engineer and characterize customized hematopoietic bone organs, here exemplified by the generation of niches overexpressing stromal-derived factor 1 alpha (SDF1α), through compositional and distributional assessment of their human cellular compartments.

The validation of the methodology bears relevance toward deciphering the human hematopoietic and skeletal systems using advanced and modular or tunable models of higher translational relevance.

RESULTS

Primary hMSCs Can Be Genetically Engineered without Altering Their Capacity to Form Hypertrophic Cartilage

Before cartilage formation, hMSCs were transduced (Figure 1A) using a VENUS (mock control) or VENUS-SDF1α lentivirus (Figure S1). The transduction allowed the generation of homogeneous VENUS and VENUS-SDF1α hMSCs populations (>93% and 96% using VENUS and VENUS-SDF1α viruses, respectively, Figure 1B). The VENUS-SDF1α transduction led to a significant SDF1α overexpression (31-fold increase in RNA levels when compared with VENUS hMSCs, Figure 1C), with transduced and untransduced MSCs displaying unchanged phenotypes (Figure S2).

Cells were subsequently seeded on collagen meshes and primed to form hyC. Over the 5-week course of *in vitro* culture, the total number of cells in the hyC remained stable (1.3×10^6 and 1.2×10^6 at weeks 1 and 5 respectively, Figure S3). During this period, the monitoring of proteins in hyC supernatant revealed comparable release profiles of angiogenic (vascular endothelial growth factor), osteoinductive (bone morphogenetic protein-2), bone remodeling (matrix metalloproteinase-13), and inflammatory (interleukin-8) factors, suggesting similar development of the templates by untransduced (primary hyC) or transduced hMSCs (VENUS and VENUS-SDF1α hyC) (Figure 1D). VENUS-SDF1α hyC secreted significantly higher amounts of SDF1α (4-fold increase at day 3, Figure 1D), although a progressive decrease was observed over time.

At the end of the *in vitro* culture, histological analysis indicated the successful formation of mature hyC in all groups, characterized by the large presence of glycosaminoglycans (safranin O, Figure 1E) and a mineralized ring at the periphery of the tissue (alizarin red, Figure 1E). Differentiation was confirmed by RT-PCR, revealing activation of chondrogenic (Collagen 2, Sox 9, Figure 1F) and hypertrophic genes (RUNX2, ALP, BSP, OSX, Figure 1F) in all hyCs. Importantly, VENUS-SDF1α hyCs were shown to maintain a marked SDF1α overexpression (Figure 1F) when compared with primary and VENUS hyCs.

Hypertrophic Cartilage with a Targeted SDF1α Enrichment Can Be Generated

After demonstrating the similar quality of hyCs and hOss derived from primary or VENUS hMSCs (Figure S4), VENUS hyCs were further used as the control group allowing for the tracing of hMSCs via the VENUS signal.

Multicolor confocal analysis of thick hyC sections was performed to investigate the presence and distribution of cells and SDF1α in the templates. VENUS cells were homogenously distributed within the tissue, largely embedded into a collagen type 2-rich matrix with detectable SDF1α proteins (Figure 2A). High-resolution imaging revealed presence of the chemokine intracellularly in both VENUS and VENUS-SDF1α cells in their corresponding hyC (Figure 2B). The SDF1α protein was also found associated with the extracellular matrix (ECM), as shown by colocalization with collagen type 2, in a more abundant fashion in VENUS-SDF1α samples (Figure 2B). To confirm microscopic observations, hyCs were lysed and assessed for their content in a panel of growth factors, including SDF1α. VENUS and VENUS-SDF1α hyCs displayed comparable protein contents (Figure 2C) except a 2-fold SDF1α enrichment in the VENUS-SDF1α templates (Figure 2C). Consistent with previous observations (Dalonneau et al., 2014; Pelletier et al., 2000), the reported decrease in secreted SDF1α over culture time (Figure 1D) can be explained by SDF1α's capacity to bind to the ECM, leading to its progressive embedding. We thus report the successful tuning of cartilage tissue's composition, through a targeted enrichment of SDF1α content.

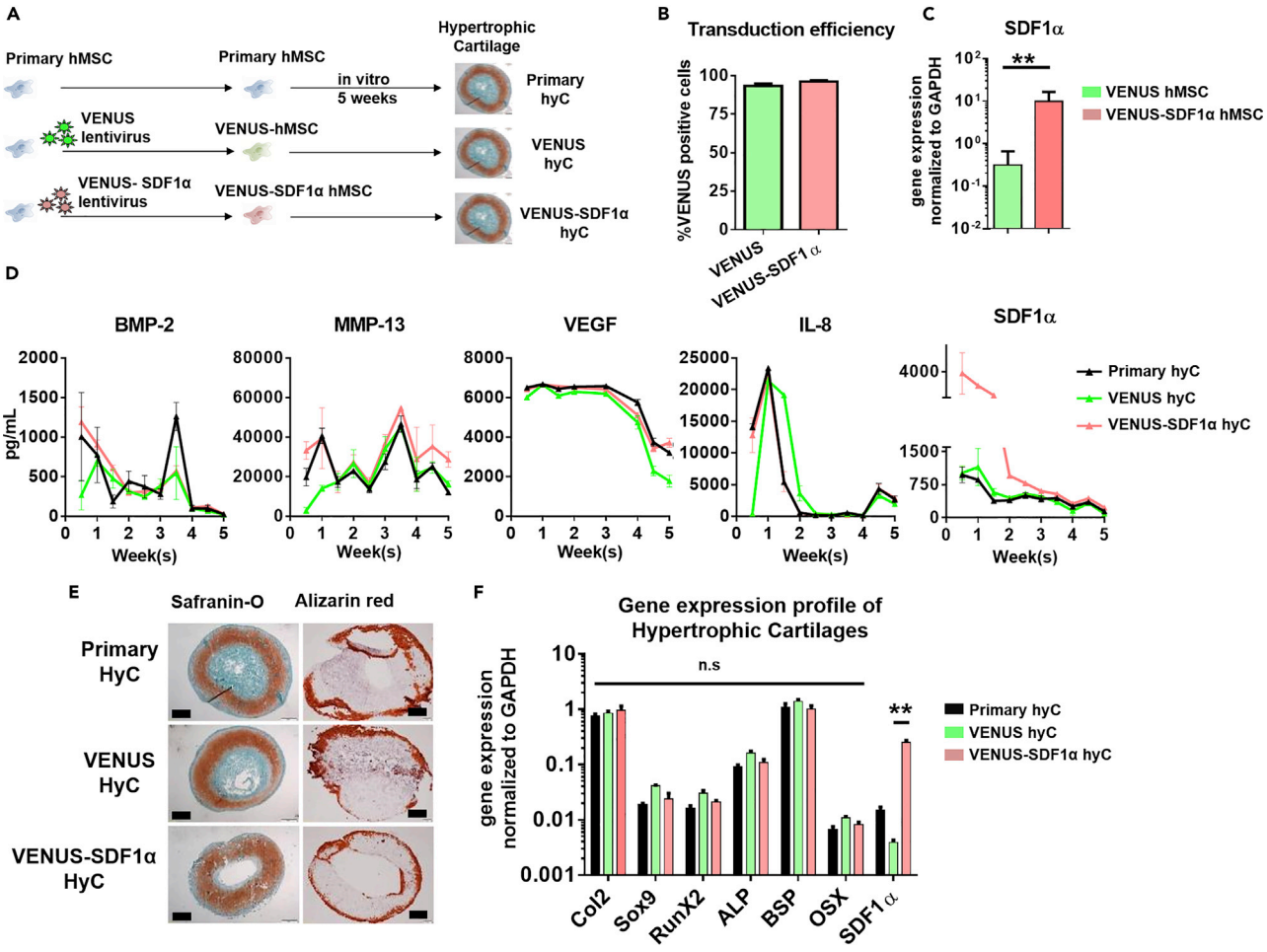

Figure 1. Primary hMSCs Can Be Genetically Engineered without Altering Their Capacity to Form Hypertrophic Cartilage

(A) Experimental design for generation of hypertrophic cartilage (hyC). SDF1α, stromal-derived factor 1 alpha.

(B) Primary hMSCs were successfully transduced with the VENUS and VENUS-SDF1α lentiviruses, as assessed by flow cytometry. n ≥ 4 biological replicates.

(C) The VENUS-SDF1α transduction led to a significantly higher expression of SDF1α levels in corresponding cells before hyC formation. **p < 0.01, using non-parametric Mann-Whitney t test. n ≥ 5 biological replicates.

(D) All hyC display similar protein secretion patterns during *in vitro* culture time, but VENUS-SDF1α hyC releases higher amounts of SDF1α. n ≥ 3 biological replicates. BMP-2, bone morphogenetic protein-2; MMP-13, matrix metalloproteinase-13; VEGF, vascular endothelial growth factor; IL-8, interleukin-8.

(E) VENUS and VENUS-SDF1α successfully displayed features of mature hypertrophic cartilage tissue following 5 weeks of *in vitro* culture, as assessed by histological analysis. Safranin O staining reveals the presence of glycosaminoglycans (red), whereas alizarin red reveals the presence of mineralized tissue (red). Scale bars, 500 μm.

(F) After 5 weeks of *in vitro* culture, VENUS-SDF1α hyC successfully displayed a typical hypertrophic molecular profile while exhibiting a significant SDF1α increase.

**p < 0.01, using one-way ANOVA. n ≥ 4 biological replicates. Col2, collagen type 2; RunX2, Runt-related transcription factor 2; ALP, alkaline phosphatase; BSP, bone sialoprotein; OSX, osterix. Data are represented as mean ± SEM.

Molecularly Engineered hyC Can Remodel into Humanized Bone Organs of Distinct Blood Compositions

In vitro-engineered VENUS and VENUS-SDF1α hyCs were subcutaneously implanted in mice (Figure 3A). After 6 weeks, when hyCs are expected to be remodeled into bone tissue, animals were intravenously transplanted with CD34+ cord-blood-derived hematopoietic cells to reconstitute human hematopoiesis (Figure 3A). After a total *in vivo* period of 12 weeks, VENUS and VENUS-SDF1α hyCs remodeled into ectopic ossicles exhibiting macroscopic evidence of vascularization (Figure 3B). Microtomography scans (Figure 3C) revealed the formation of mature bone tissue with no quality differences between the two hOss types, consisting in a spheroid organ of 18 ± 2.1 mm^3 (Figure S5). Confocal microscopy allowed to identify

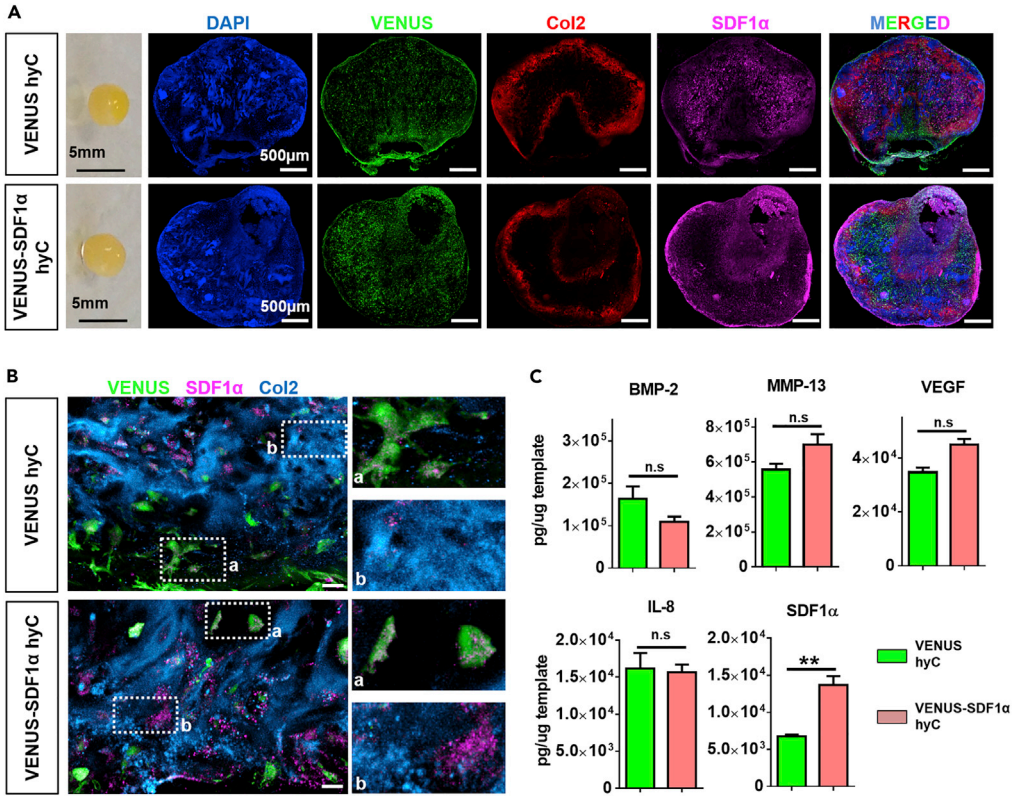

Figure 2. Hypertrophic Cartilage with a Targeted SDF1α Enrichment Can Be Generated

(A) VENUS and VENUS-SDF1α hyC consist in cartilage pellets (macroscopic view, left) in which hMSCs (VENUS positive) and the SDF1α protein are found abundantly in the collagen-rich matrix, as assessed by immunofluorescence analysis of thick hyC sections. Col2, collagen type 2. Scale bars, 500 μm.

(B) SDF1α is more abundant in the ECM of VENUS-SDF1α hyC, as revealed by high-resolution immunofluorescent imaging. Scale bars, 20 μm. Col2, collagen type 2.

(C) A significant and specific SDF1α enrichment is obtained in the VENUS-SDF1α hyC, as assessed by protein quantification. n = 3 biological repeats. **p < 0.01, using one-way ANOVA test. Data are represented as mean ± SEM.

human blood cells in the hOss, forming heterogeneous "islets" of human hematopoiesis, indicating successful engraftment (Figure 3D).

Human blood populations were quantified by flow cytometry in retrieved hOss and corresponding mouse bones (Figures S6A and S6B). Engraftment of human blood cells was similar with an average hCD45 chimerism level of 40% (Figure 3E). VENUS hOss and mouse bones displayed comparable frequencies of naive and more committed blood populations (Figures 3E and S6C), whereas hOss overexpressing SDF1α showed significantly higher frequencies of multipotent progenitors (MPPs) and common myeloid progenitors (CMPs)/megakaryocyte-erythroid progenitor (MEPs) (2.7- and 2.4-fold increase, respectively) and superior HSPC and HSC content (1.8- and 1.9-fold increase, respectively), although not reaching significance.

The functionality of hCD45/CD34+ cells retrieved from mouse bones or hOss was evaluated by *in vitro* colony formation unit (CFU) assays. Cells were capable of efficiently giving rise to all myeloid colonies, but the hCD45/CD34+ fraction derived from hOss displayed a significantly higher potential to form hematopoietic colonies, including GEmM, than the corresponding population retrieved from mouse bones (Figure S6D). No differences in CFU activity were observed between cells retrieved from VENUS or VENUS-SDF1α hOss, suggesting that the SDF1α overexpression did not affect stem and progenitor functionalities. We thus validate the generation of SDF1α-customized hOss, composed of an increased frequency of HSPCs without alterations of their functionality.

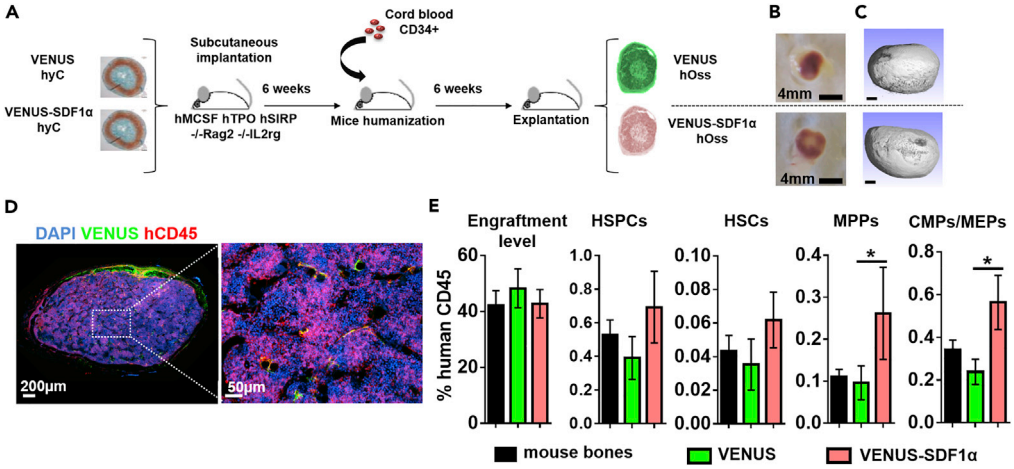

Figure 3. Molecularly Engineered hyC Can Remodel into Humanized Bone Organs of Distinct Blood Compositions

(A) Experimental design for the generation of humanized ossicles (hOss). Engineered hyCs are implanted into immunocompromised animals. Mice are humanized 6 weeks later by intravenous transplantation of human CD34+ isolated from cord blood. Constructs are retrieved 6 weeks later for analysis.

(B and C) (B) VENUS and VENUS-SDF1α hyCs successfully remodeled into ossicles, as shown macroscopically by blood colonization and (C) by microtomographic scans revealing the formation of mature bone tissue. Ossicles were retrieved after 12 weeks *in vivo*. Scale bars, 0.5 mm.

(D) Humanized ossicles display a chimeric blood composition organized in "islets" of human hematopoieisis.

(E) SDF1α-overexpressing ossicles displayed higher frequencies of human blood populations, as assessed by flow cytometry. $n \geq 18$ biological replicates from four independent experiments. *$p < 0.5$, using one-way ANOVA test. CMPs, common myeloid progenitors; HSCs, hematopoietic stem cells; HSPCs, hematopoietic stem and progenitor cells; MEPs, megakaryocyte-erythroid progenitors; MPPs, multipotent progenitors. Data are represented as mean ± SEM.

Quantitative Microscopy of Bone Organs Reveals the Reconstitution of a Human Mesenchymal Niche including Rare Mesenchymal-Hematopoietic Physical Interactions

Deep confocal analysis on both types of hOss offered a quantitative understanding of the reconstituted BM environment. Serial sectioning of hOss allowed gathering comprehensive 3D information (Figures 4A and S7A) and indicated an intense vascularization surrounding the hOss with its cavity largely filled by BM cells. The hOss were also connected to the host nervous system as shown by evidences of innervation (peripherin, Figure S7B).

The presence of hMSCs in both VENUS and VENUS-SDF1α organs was identified by VENUS expression (Figure S8A). The segmentation of VENUS cells (Figure S8A) in corresponding sections (Figure S8B) allowed determining the average number of hMSCs per hOss. From the 1.2×10^6 hMSCs present in the hyC at the time of implantation, only 0.1×10^6 were still populating the hOss, corresponding to a 90% decrease (Figure S8C). To corroborate this finding, flow cytometry quantification of VENUS cells after hOss digestion was also performed, giving a number of hMSCs per hOss of 0.06×10^6 (Figure S8C). The difference is likely due to difficulty to retrieve bone-embedded hMSCs and adipocytes. The observed hMSC death was not due to the animal irradiation, because non-irradiated hOss gave similar numbers (0.07×10^6, Figure S8C).

Remarkably, in the engineered hOss, hMSCs were associated with an important fate diversity following the remodeling of hyC. HMSCs' fates in bone organs were quantified by specific segmentation strategies (c.f. Methods section and Figures S8 and S9). First, no significant differences could be observed between VENUS and VENUS-SDF1α hOss, indicating that the hMSCs' genetic modification did not impact their subsequent fate decisions upon hOss formation. The capacity to manipulate hMSCs without impairing their endochondral program allows the stringent assessment of SDF1α effects. As such, the previously observed distinct human blood composition in VENUS-SDF1α hOss can be strictly attributed to the factor overexpression.

In all hOss, hMSCs were abundantly found within the BM stroma (stromal, 45% and 47% in VENUS and VENUS-SDF1α hOss respectively, Figure 4B), exhibiting a fibroblast-like shape and positivity for CD90 (Figure S9A). A large fraction of them (47% and 50%, respectively; Figure 4B) was directly associated with vasculature (0–1 μm distance to vessels). The hMSCs' enrichment at vessel sites was confirmed by comparison to

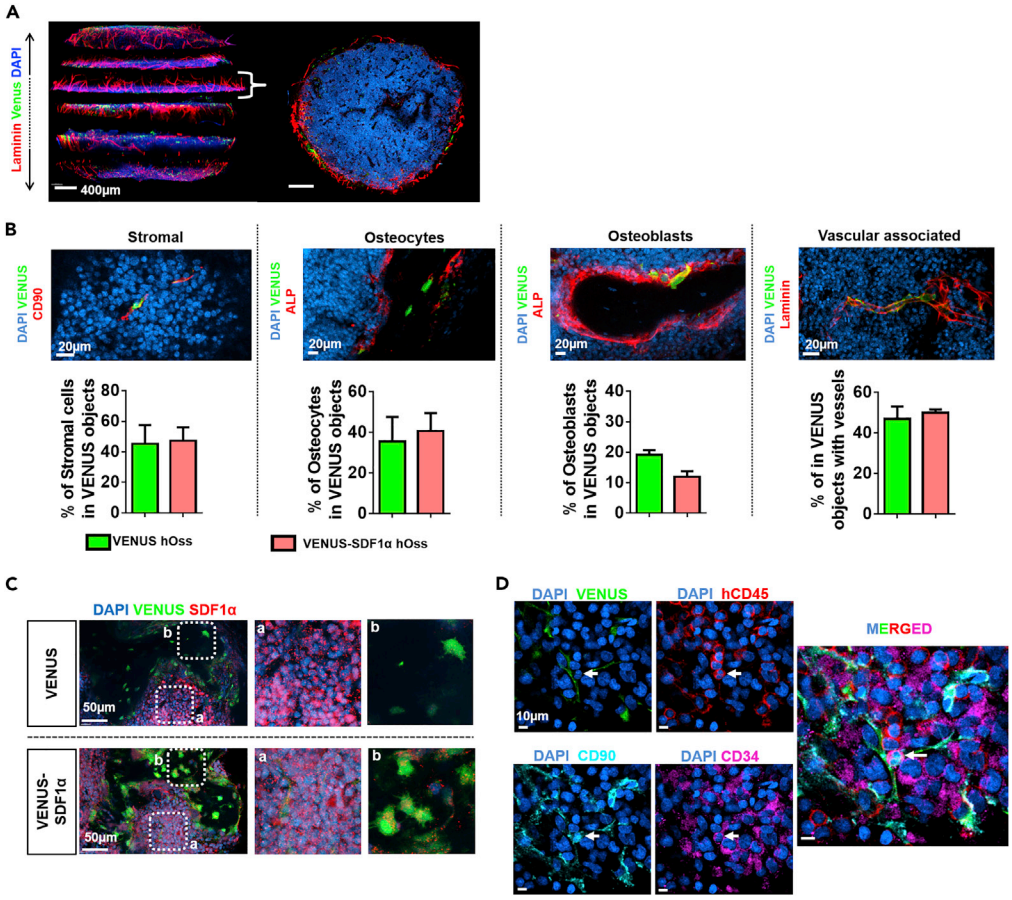

Figure 4. Quantitative Microscopy of Bone Organs Reveals the Reconstitution of a Human Mesenchymal Niche Including Rare Mesenchymal-Hematopoietic Physical Interactions

(A) Multidimensional confocal immunofluorescence imaging allows for the reconstitution of hOss for 3D quantitative information retrieval (left). Top view of a transverse hOss section (right) illustrating the internal bone marrow cavity (DAPI) and intense peripheral vascularization (lamimin). Scale bars, 400 µm.

(B) Top: implanted hMSCs (VENUS positive) demonstrate fate plasticity by acquiring multiple niche cell phenotypes. Scale bars, 20 µm. Bottom: fate quantification of VENUS hMSCs based on the segmentation of immunofluorescence data. Stromal cells, venus+/CD90+/stroma localization; osteocytes, venus+/ALP-/localization in bone nodules; osteoblasts, venus+/ALP+/localization at the bone and bone marrow interface; vascular associated, venus+/distance to lamimin+ vessels < 1 µm; ALP, alkaline phosphatase. n ≥ 3 biological replicates.

(C) The SDF1α protein was expressed by blood cells and also found more abundantly in VENUS cells from the VENUS-SDF1α ossicles. Right and b are magnification panels.

(D) Deep confocal analysis of hOss allows for the identification and localization of a rare HSPC subset (arrow, hCD45/CD34/CD90), found directly in contact with hMSC-derived niche cells. n = 10 events detected in 5.9 mm^3 of tissue scanned. Data are represented as mean ± SEM.

a random dots distribution (Figure S9C). HMSCs also differentiated into the osteogenic lineage in the form of osteocytes embedded in the bone matrix (osteocytes, Figures 4B and S9A), accounting for 36% (VENUS hOss) and 41% (VENUS-SDF1α hOss) of total VENUS cells. Lining osteoblasts were less abundant (19% in VENUS hOss versus 12% in VENUS-SDF1α hOss, Figures 4B and S9A). To a lower extent, we also identified hMSCs differentiated into the adipogenic lineage, as shown by the presence of VENUS-positive adipocytes (Figure S7D).

To obtain a better understanding of the observed *in vivo* fate diversity, we further investigated the proportion of hMSCs committed to certain lineages before implantation, at the hyC stage (5 weeks *in vitro* culture). The Sox-9 and RUNX2 transcription factors are typically associated with chondrogenic (Akiyama et al., 2002) and osteoblastic (Ducy et al., 1997) differentiation, respectively; 41.3% (±5.6) of the cells

were positive for Sry-box 9 (Sox-9), 6.3% (±5) expressed the Runt-related transcription factor 2 (RUNX2), and 10.8% (±5.6) were both RUNX2 and Sox-9 positive (Figure S10). No cells showed positivity for the adipocytic marker peroxisome proliferator-activated receptor gamma (Lefterova et al., 2014). As such, the majority of our cells were chondrocytes (Sox-9 positivity), hypertrophic chondrocytes (Sox-9 and/or RUNX2 positivity), or osteoblasts (RUNX2 positivity). Interestingly, despite the 5-week course of differentiation, 29.9% ± 1.6% maintained the expression of Stro-1, a progenitor marker associated with multipotency (Lin et al., 2011). This indicates that some hMSCs are not fully committed at the end of the *in vitro* differentiation stage and acquire their definitive function after implantation.

Further immunofluorescence analysis of the ossicles was performed. SDF1α staining revealed the presence of the protein in the marrow (Figure 4C), expressed by blood cells (Dar et al., 2006). The SDF1α protein could also be detected in hMSCs-derived cells from VENUS-SDF1α hOss (Figure 4C). Acquisition of deep multicolor staining was further performed for the identification of hMSC-derived niche cells (positive for VENUS) and particular HSPC populations within engineered hOss. This allowed the localization of a very rare subset of HSPCs (hCD45+/CD34+/CD90+) described to be enriched for functional HSCs, which was consistently in physical contact (less than 1 μm distance) with VENUS cells, in both VENUS and VENUS-SDF1α niches (n = 10 events detected in 5.9 mm^3 of tissue scanned, Figure 4D). To ensure that those interactions did not result from a random distribution, we investigated the probability for HSPCs touching an hMSC (Figure S11). This probability was found to be 36% (±11), although 100% of the HSPCs we found were in contact with hMSCs.

This recurrent physical interaction between the human stromal and naive hematopoietic compartments, combined with the finding that SDF1α customization leads to changes in frequencies of hematopoietic populations, supports a functional contact-triggered regulation of HSPCs by the human mesenchymal compartment, to date only reported in mouse studies (Gomariz et al., 2018; Rongvaux et al., 2011).

DISCUSSION

We report the engineering and characterization of customized human hematopoietic bone organs. The method relies on the genetic modification of primary hMSCs, their priming to recapitulate the developmental program of endochondral ossification (Kronenberg and Kronenberg, 2003), and quantitative multidimensional imaging of the reconstituted human BM environment.

The study of hematopoiesis in a humanized context is a primary challenge. The generation of transgenic animals supporting human engraftment is associated with some limitations (Devoy et al., 2012), including time-consuming single-gene targeting, the unpredictable biological outcome (e.g., embryonic lethality, low efficiency, absence of recognizable phenotypes), and the often non-tissue-specific nature if at all conditional. Instead, our strategy relies on the exploitation and characterization of the hOss model, using hMSCs as cellular vectors for the targeted delivery of factors influencing the composition of the human blood compartment. The introduced modification is thus confined within the BM tissue as ensured by hMSC-derived niche cells.

The biological validation of the method was performed using SDF1α as a known factor influencing stem cell behavior. SDF1α has been reported both as stem cell chemoattractant (Aiuti et al., 1997; Lapidot and Kollet, 2002; Mohle et al., 1998) and pro-quiescent molecule (Itkin and Lapidot, 2011; Tzeng et al., 2011), thus offering multiple readouts to validate the effects of its overexpression in hOss. Pre-existing molecular engineering approach (Carretta et al., 2017; Chen et al., 2012) models did not investigate the effect of the genetic modification on the reconstituted human niche environment. As a direct consequence, impact on the blood compartment could not be strictly attributed to the factor's secretion. Here, the SDF1α overexpression was shown to specifically affect the human blood composition while not affecting the fate and distribution of implanted hMSCs. The capacity to manipulate hMSCs without impairing their endochondral program is a pre-requisite for the direct assessment of SDF1α effects. We observed a specific enrichment in CMPs/MEPs, MPPs, and HSC populations in SDF1α-overexpressing hOss. All these populations express the CXCR4 receptor (Toni et al., 2011), thus being sensitive to the SDF1α chemoattractant effect (Peled et al., 1999). The previously reported SDF1α-driven mobilization of CD34+ cells by stromal cells included the recruitment of more committed erythroid, lymphoid, and myeloid lineages (Bleul et al., 2002). Our observations are thus in line with the existing literature, although our study is the first exploiting a humanized approach to evidence an SDF1α-triggered effect. Although our model was previously validated for the engraftment of fully functional HSCs (Fritsch et al., 2018), secondary transplantation would be required to assess putative SDF1α effects on the self-renewal of long-term repopulating stem cells.

Interestingly, the association of SDF1α with proteoglycans—the main constituents of cartilaginous ECM (Roughley and Lee, 1994)—was reported to strongly promote the migration of HSPCs (Netelenbos et al., 2002). This might suggest that the observed effects result from preferential homing at the time of engraftment (Lapidot and Kollet, 2002), although a different cycling rate of HSPCs cannot be excluded.

In our study, we used advanced microscopy tools to monitor hMSCs within the engineered tissues, from the *in vitro* hyC stage to the fully remodeled hOss. As easily accessible organs tunable in size, quantitative 3D information on the hOss cellular composition could be retrieved and offered a comprehensive understanding of the human niche in this *in vivo* setting. This revealed a remarkable degree of hMSCs' plasticity in the model, giving rise to several niche phenotypes, including lining osteoblasts, osteocytes, stromal cells, and adipocytes. Distance analyses indicated not only a strong association of hMSCs with vasculature but also direct physical interactions with HSPCs. The observed fate diversity may derive from a pool of hMSCs with no signs of chondrogenic or osteoblastic commitment at the hyC stage. However, lineage-committed hMSCs have also been described as capable of transdifferentiation (Song and Tuan, 2004).

Although previous studies reported the presence of hMSCs in ossicles (Abarrategi et al., 2017; Martine et al., 2017; Reinisch et al., 2016), their functional status has not been rigorously demonstrated beyond their support for human blood engraftment. Our work evidences for the first time a functional regulatory role of hMSCs in the model, validated by the SDF1α customization leading to distinct changes in frequencies of hematopoietic populations. These were achieved despite the relatively low number of hMSCs composing the niche and supporting human blood cell engraftment. Collectively, these findings reinforce the notion that hMSCs are essential niche players (Méndez-Ferrer et al., 2010; Morrison and Scadden, 2014) in the engineered ossicles and support a contact-triggered regulation of HSPCs by the mesenchymal compartment, only previously reported in mouse studies (Rongvaux et al., 2011). The detection of a high number of interactions of a more specific HSC phenotype (CD45+/CD34+/CD38-/CD45RA-/CD90+/CD49f+) (Fares et al., 2014), which requires challenging immunofluorescence multiplexing, would, however, be required to provide direct evidence of a physical interaction between hMSCs and functional HSCs.

The functional role of hMSCs in the hOss model supports their use for the molecular engineering of human niches. The importance of the proximity between hMSCs and HSPCs could be further evaluated by overexpression of signaling molecules requiring direct contact of adjacent cells for influencing their fate decisions, e.g., Notch ligands (Artavanis-Tsakonas et al., 1999). The paradigm of customization can also be further explored with additional factors putatively affecting stem cell homing/localization/function in pathological scenarios (e.g., by engraftment of leukemic primary material) and include the impact assessment on the human niche compartment. In fact, the hOss could be valuable for the identification of specific human niche cell populations, derived from the implanted hMSCs. This is of particular importance in pathologic scenarios, in which the role of the stroma and associated factors in disease evolution remains elusive (Schepers et al., 2015, 2013). Our model could thus help deciphering the complex phenotypes and functions associated with hMSCs (Mo et al., 2016; Nombela-Arrieta et al., 2011) in myeloid or lymphoid malignancies. Along the same line, our model could also be exploited to study the engraftment of metastatic solid tumors (e.g., breast, prostate) that naturally migrate to bones, including those for which SDF1α has been shown to be highly expressed in BM sites of tumor metastasis (Roccaro et al., 2014).

Toward these objectives, the exploitation of dedicated cell lines may not only facilitate molecular engineering of hMSCs but also potentially lead to their higher survival in the BM. This would maximize the therapeutic delivery of factors impacting engrafted healthy or malignant blood populations. However, so far no hMSC line was proved capable of recapitulating the endochondral process.

Finally, using similar knockout or knockin strategies in hMSCs, we also envision the possibility of identifying key molecular players of the endochondral program, by studying their impact on hMSC fate decision. The ossicle would thus be exploited as a developmental model of human bone formation.

Limitations of the Study

For immunofluorescence analysis, the hCD45+/CD34+/CD90 + phenotype was used to identify HSPCs. Of this population, 24.6% are CD34+/CD38-/CD45RA-CD90+, of which 5% were reported to be functional HSCs in freshly isolated cord blood (Notta et al., 2011). The hCD45+/CD34+/CD90 + population thus contains ca. 1.2% functional HSCs. Detection of functional HSCs will require improved HSC markers. In

addition, owing to the large required effort, only a small number of these cells were imaged in ossicles. A higher number will allow robust statistical analysis of human MSC-HSPC interactions.

METHODS

All methods can be found in the accompanying Transparent Methods supplemental file.

SUPPLEMENTAL INFORMATION

Supplemental Information can be found online at https://doi.org/10.1016/j.isci.2019.08.006.

ACKNOWLEDGMENTS

This study was supported in part by the SystemsX (StemSysMed grant #2014/266 to M.G.M., T.S., and I.M.) and Division III Programs (grant # 31003A_156430 to I.M.) of the Swiss National Science Foundation.

AUTHOR CONTRIBUTIONS

P.E.B., I.M., T.S., and M.G.M. designed the research. P.E.B., K.F., and S.P. performed experiments. P.E.B., K.F., S.P., H.T., L.K., K.D.K., and D.L.C. analyzed data. P.E.B., T.S., I.M., and M.G.M. wrote the manuscript. P.E.B., T.S., I.M., and M.G.M. financed the project.

DECLARATION OF INTERESTS

The authors declare no competing interests.

Received: December 16, 2018
Revised: July 1, 2019
Accepted: August 2, 2019
Published: September 27, 2019

REFERENCES

Abarrategi, A., Foster, K., Hamilton, A., Mian, S.A., Passaro, D., Gribben, J., Mufti, G., and Bonnet, D. (2017). Versatile humanized niche model enables study of normal and malignant human hematopoiesis. J. Clin. Invest. *127*, 543–548.

Aiuti, A., Webb, I.J., Bleul, C., Springer, T., and Gutierrez-Ramos, J.C. (1997). The chemokine SDF-1 is a chemoattractant for human CD34+ hematopoietic progenitor cells and provides a new mechanism to explain the mobilization of CD34+ progenitors to peripheral blood. J. Exp. Med. *185*, 111–120.

Akiyama, H., Chaboissier, M.C., Martin, J.F., Schedl, A., and De Crombrugghe, B. (2002). The transcription factor Sox9 has essential roles in successive steps of the chondrocyte differentiation pathway and is required for expression of Sox5 and Sox6. Genes Dev. *16*, 2813–2828.

Antonelli, A., Noort, W.A., Jaques, J., de Boer, B., de Jong-Korlaar, R., Brouwers-Vos, A.Z., Lubbers-Aalders, L., van Velzen, J.F., Bloem, A.C., Yuan, H., et al. (2016). Establishing human leukemia xenograft mouse models by implanting human bone marrow-like scaffold-based niches. Blood *128*, 2949–2959.

Artavanis-Tsakonas, S., Rand, M.D., and Lake, R.J. (1999). Notch signaling: cell fate control and signal integration in development. Science *284*, 770–776.

Bleul, C., Webb, I.J., Springer, T., Gutierrez-Ramos, J.C., and Aiuti, A. (2002). The chemokine SDF-1 is a chemoattractant for human CD34 + hematopoietic progenitor cells and provides a new mechanism to explain the mobilization of CD34 + progenitors to peripheral blood. J. Exp. Med.. https://doi.org/10.1084/jem.185.1.111

Bourgine, P.E., Martin, I., and Schroeder, T. (2018). Engineering human bone marrow proxies. Cell Stem Cell *22*, 298–301.

Bourgine, P.E., Scotti, C., Pigeot, S., Tchang, L.A., Todorov, A., and Martin, I. (2014). Osteoinductivity of engineered cartilaginous templates devitalized by inducible apoptosis. Proc. Natl. Acad. Sci. U S A *111*, 17426–17431.

Carretta, M., de Boer, B., Jaques, J., Antonelli, A., Horton, S.J., Yuan, H., de Bruijn, J.D., Groen, R.W.J., Vellenga, E., and Schuringa, J.J. (2017). Genetically engineered mesenchymal stromal cells produce IL-3 and TPO to further improve human scaffold-based xenograft models. Exp. Hematol. *51*, 36–46.

Chen, Y., Jacamo, R., Shi, Y.X., Wang, R.Y., Battula, V.L., Konoplev, S., Strunk, D., Hofmann, N.A., Reinisch, A., Konopleva, M., and Andreeff, M. (2012). Human extramedullary bone marrow in mice: a novel in vivo model of genetically controlled hematopoietic microenvironment. Blood *119*, 4971–4980.

Coutu, D.L., Kokkaliaris, K.D., Kunz, L., and Schroeder, T. (2017). Three-dimensional map of non-hematopoetic bone and bone marrow cells and molecules. Nat. Biotechnol. *35*, 1202–1210.

Dalonneau, F., Liu, X.Q., Sadir, R., Almodovar, J., Mertani, H.C., Bruckert, F., Albiges-Rizo, C., Weidenhaupt, M., Lortat-Jacob, H., and Picart, C. (2014). The effect of delivering the chemokine SDF-1α in a matrix-bound manner on myogenesis. Biomaterials *35*, 4525–4535.

Dar, A., Kollet, O., and Lapidot, T. (2006). Mutual, reciprocal SDF-1/CXCR4 interactions between hematopoietic and bone marrow stromal cells regulate human stem cell migration and development in NOD/SCID chimeric mice. Exp. Hematol. *34*, 967–975.

Devoy, A., Bunton-Stasyshyn, R.K.A., Tybulewicz, V.L.J., Smith, A.J.H., and Fisher, E.M.C. (2012). Genomically humanized mice: technologies and promises. Nat. Rev. Genet. *13*, 14–20.

Doulatov, S., Notta, F., Laurenti, E., and Dick, J.E. (2012). Hematopoiesis: a human perspective. Cell Stem Cell *10*, 120–136.

Ducy, P., Zhang, R., Geoffroy, V., Ridall, A.L., and Karsenty, G. (1997). Osf2/Cbfa1: a transcriptional activator of osteoblast differentiation. Cell *89*, 747–754.

Engler, A.J., Sen, S., Sweeney, H.L., and Discher, D.E. (2006). Matrix elasticity directs stem cell lineage specification. Cell *126*, 677–689.

Fares, I., Chagraoui, J., Gareau, Y., Gingras, S., Ruel, R., Mayotte, N., Csaszar, E., Knapp, D.J.H.F., Miller, P., Ngom, M., et al. (2014). Pyrimidoindole derivatives are agonists of human hematopoietic stem cell self-renewal. Science *345*, 1509–1512.

Fritsch, K., Pigeot, S., Feng, X., Bourgine, P.E., Schroeder, T., Martin, I., Manz, M.G., and Takizawa, H. (2018). Engineered humanized bone organs maintain human hematopoiesis in vivo. Exp. Hematol. *61*, 45–51.e5.

Gomariz, A., Helbling, P.M., Isringhausen, S., Suessbier, U., Becker, A., Boss, A., Nagasawa, T., Paul, G., Goksel, O., Székely, G., et al. (2018). Quantitative spatial analysis of haematopoiesis-regulating stromal cells in the bone marrow microenvironment by 3D microscopy. Nat. Commun. *9*, 2532.

Guilak, F., Cohen, D.M., Estes, B.T., Gimble, J.M., Liedtke, W., and Chen, C.S. (2009). Control of stem cell fate by physical interactions with the extracellular matrix. Cell Stem Cell *5*, 17–26.

Itkin, T., and Lapidot, T. (2011). SDF-1 keeps HSC quiescent at home. Blood *117*, 373–374.

Keung, A.J., Healy, K.E., Kumar, S., and Schaffer, D.V. (2010). Biophysics and dynamics of natural and engineered stem cell microenvironments. Wiley Interdiscip. Rev. Syst. Biol. Med. *2*, 49–64.

Knapp, D.J.H.F., Hammond, C.A., Aghaeepour, N., Miller, P.H., Pellacani, D., Beer, P.A., Sachs, K., Qiao, W., Wang, W., Humphries, R.K., et al. (2016). Distinct signaling programs control human hematopoietic stem cell survival and proliferation. Blood *129*, 307–319.

Kronenberg, H.M., and Kronenberg, H.M. (2003). Developmental regulation of the growth plate. Nature *423*, 332–336.

Kunisaki, Y., and Frenette, P.S. (2012). The secrets of the bone marrow niche: enigmatic niche brings challenge for HSC expansion. Nat. Med. *18*, 864–865.

Lapidot, T., and Kollet, O. (2002). The essential roles of the chemokine SDF-1 and its receptor CXCR4 in human stem cell homing and repopulation of transplanted immune-deficient NOD/SCID and NOD/SCID/B2mnull mice. Leukemia *16*, 1992–2003.

Lefterova, M.I., Haakonsson, A.K., Lazar, M.A., and Mandrup, S. (2014). PPARγ and the global map of adipogenesis and beyond. Trends Endocrinol. Metab. *25*, 293–302.

Lin, G., Liu, G., Banie, L., Wang, G., Ning, H., Lue, T.F., and Lin, C.-S. (2011). Tissue distribution of mesenchymal stem cell marker stro-1. Stem Cells Dev. *20*, 1747–1752.

Martine, L.C., Holzapfel, B.M., McGovern, J.A., Wagner, F., Quent, V.M., Hesami, P., Wunner, F.M., Vaquette, C., De-Juan-Pardo, E.M., Brown, T.D., et al. (2017). Engineering a humanized bone organ model in mice to study bone metastases. Nat. Protoc. *12*, 639–663.

Méndez-Ferrer, S., Michurina, T.V., Ferraro, F., Mazloom, A.R., Macarthur, B.D., Lira, S.A., Scadden, D.T., Ma'ayan, A., Enikolopov, G.N., and Frenette, P.S. (2010). Mesenchymal and haematopoietic stem cells form a unique bone marrow niche. Nature *466*, 829–834.

Mo, M., Wang, S., Zhou, Y., Li, H., and Wu, Y. (2016). Mesenchymal stem cell subpopulations: phenotype, property and therapeutic potential. Cell. Mol. Life Sci. *73*, 3311–3321.

Mohle, R., Bautz, F., Rafii, S., Moore, M.A., Brugger, W., and Kanz, L. (1998). The chemokine receptor CXCR-4 is expressed on CD34+ hematopoietic progenitors and leukemic cells and mediates transendothelial migration induced by stromal cell-derived factor-1. Blood *91*, 4523–4530.

Morrison, S.J., and Scadden, D.T. (2014). The bone marrow niche for haematopoietic stem cells. Nature *505*, 327–334.

Netelenbos, T., Zuijderduijn, S., Van Den Born, J., Kessler, F.L., Zweegman, S., Huijgens, P.C., and Dräger, A.M. (2002). Proteoglycans guide SDF-1-induced migration of hematopoietic progenitor cells. J. Leukoc. Biol. *72*, 353–362.

Nombela-Arrieta, C., Ritz, J., and Silberstein, L.E. (2011). The elusive nature and function of mesenchymal stem cells. Nat. Rev. Mol. Cell Biol. *12*, 126–131.

Notta, F., Doulatov, S., Laurenti, E., Poeppl, A., Jurisica, I., and Dick, J.E. (2011). Isolation of single human hematopoietic stem cells capable of long-term multilineage engraftment. Science *333*, 218–221.

Peled, A., Petit, I., Kollet, O., Magid, M., Ponomaryov, T., Byk, T., Nagler, A., Ben-Hur, H., Many, A., Shultz, L., et al. (1999). Dependence of human stem cell engraftment and repopulation of NOD/SCID mice on CXCR4. Science *283*, 845–848.

Pelletier, A.J., van der Laan, L.J.W., Hildbrand, P., Siani, M.A., Thompson, D.A., Dawson, P.E., Torbett, B.E., and Salomon, D.R. (2000). Presentation of chemokine SDF-1α by fibronectin mediates directed migration of T cells. Blood *96*, 2682–2690.

Reinisch, A., Thomas, D., Corces, M.R., Zhang, X., Gratzinger, D., Hong, W.-J., Schallmoser, K., Strunk, D., and Majeti, R. (2016). A humanized bone marrow ossicle xenotransplantation model enables improved engraftment of healthy and leukemic human hematopoietic cells. Nat. Med. *22*, 812–821.

Rieger, M.A., Hoppe, P.S., Smejkal, B.M., Eitelhuber, A.C., and Schroeder, T. (2009). Hematopoietic cytokines can instruct lineage choice. Science *325*, 217–218.

Roccaro, A.M., Sacco, A., Purschke, W.G., Moschetta, M., Buchner, K., Maasch, C., Zboralski, D., Zöllner, S., Vonhoff, S., Mishima, Y., et al. (2014). SDF-1 inhibition targets the bone marrow niche for cancer therapy. Cell Rep. *9*, 118–128.

Rongvaux, A., Willinger, T., Martinek, J., Strowig, T., Gearty, S.V., Teichmann, L.L., Saito, Y., Marches, F., Halene, S., Palucka, A.K., et al. (2014). Development and function of human innate immune cells in a humanized mouse model. Nat. Biotechnol. *32*, 364–372.

Rongvaux, A., Willinger, T., Takizawa, H., Rathinam, C., Auerbach, W., Murphy, A.J., Valenzuela, D.M., Yancopoulos, G.D., Eynon, E.E., Stevens, S., et al. (2011). Human thrombopoietin knockin mice efficiently support human hematopoiesis in vivo. Proc. Natl. Acad. Sci. U S A *108*, 2378–2383.

Roughley, P.J., and Lee, E.R. (1994). Cartilage proteoglycans: structure and potential functions. Microsc. Res. Tech. *28*, 385–397.

Schepers, K., Campbell, T.B., and Passegué, E. (2015). Normal and leukemic stem cell niches: insights and therapeutic opportunities. Cell Stem Cell *16*, 254–267.

Schepers, K., Pietras, E.M., Reynaud, D., Flach, J., Binnewies, M., Garg, T., Wagers, A.J., Hsiao, E.C., and Passegué, E. (2013). Myeloproliferative neoplasia remodels the endosteal bone marrow niche into a self-reinforcing leukemic niche. Cell Stem Cell *13*, 285–299.

Scotti, C., Piccinini, E., Takizawa, H., Todorov, A., Bourgine, P., Papadimitropoulos, A., Barbero, A., Manz, M.G., and Martin, I. (2013). Engineering of a functional bone organ through endochondral ossification. Proc. Natl. Acad. Sci. U S A *110*, 3997–4002.

Song, L., and Tuan, R.S. (2004). Transdifferentiation potential of human mesenchymal stem cells derived from bone marrow. FASEB J. *18*, 980–982.

Toni, R., Tampieri, A., Zini, N., Strusi, V., Sandri, M., Dallatana, D., Spaletta, G., Bassoli, E., Gatto, A., Ferrari, A., and Martin, I. (2011). Ex situ bioengineering of bioartificial endocrine glands: a new frontier in regenerative medicine of soft tissue organs. Ann. Anat. *193*, 381–394.

Tzeng, Y.S., Li, H., Kang, Y.L., Chen, W.G., Cheng, W., and Lai, D.M. (2011). Loss of Cxcl12/Sdf-1 in adult mice decreases the quiescent state of hematopoietic stem/progenitor cells and alters the pattern of hematopoietic regeneration after myelosuppression. Blood *117*, 429–439.

van Pel, M., Fibbe, W.E., and Schepers, K. (2015). The human and murine hematopoietic stem cell niches: are they comparable? Ann. N. Y. Acad. Sci. *1370*, 55–64.

Zhang, C.C., and Lodish, H.F. (2008). Cytokines regulating hematopoietic stem cell function. Curr. Opin. Hematol. *15*, 307–311.

ISCI, Volume *19*

Supplemental Information

Fate Distribution and Regulatory Role of Human Mesenchymal Stromal Cells in Engineered Hematopoietic Bone Organs

Paul E. Bourgine, Kristin Fritsch, Sebastien Pigeot, Hitoshi Takizawa, Leo Kunz, Konstantinos D. Kokkaliaris, Daniel L. Coutu, Markus G. Manz, Ivan Martin, and Timm Schroeder

Transparent Methods section

Isolation and culture of hMSCs

All experiments were conformed to the regulatory standards of the ETH Zurich, the University Hospital of Basel and the University of Zürich. hMSCs were isolated from human BM aspirates from the iliac crest, after ethical approval (EKBB, Ref. 78/07) and informed donor consent from patients. Bone marrow aspirates (20 mL volume) were harvested from healthy donors (N≥3, females and males 30 to 65 years old) using a biopsy needle inserted through the cortical bone, and immediately transferred into plastic tubes containing 15,000 IU heparin. After diluting the marrow aspirates with phosphate buffered saline (PBS) at a ratio of 1:4, nucleated cells were isolated using a density gradient solution (Histopaque, Sigma Chemical, Buchs, CH). Complete medium consisting in α-minimum essential Medium (αMEM) with 10% fetal bovine serum, 1% HEPES (1 M), 1% sodium pyruvate (100 mM) and 1% of Penicillin–Streptomycin– Glutamine (100X) solution (all from Gibco). Nucleated cells were plated at a density of 33×10^6 cells/cm3 in complete medium supplemented with 5 ng/ml of fibroblast growth factor-2 (FGF-2, R&D Systems) and cultured in a humidified 37 °C/5% CO_2 incubator. Medium was changed twice in a week. HMSCs were selected on the basis of adhesion and proliferation on the plastic substrate one week after seeding. In this study, donors were pre-selected based on their capacity to differentiate *in vitro* into the chondrogenic lineage.

Plasmid constructs

The lentivector VENUS-SDF1 was obtained by cloning the SDF1α gene extracted from the pBABE puro SDF-1 alpha plasmid (Addgene, plasmid #12270) was cloned by restriction digest into a third generation lentiviral backbone (Schambach et al., 2006) containing the VENUS transgene. The VENUS lentivector consisted in the same system without the SDF1α gene.

Virus production and hMSC transductions

Third generation vesicular stomatitis virus glycoprotein (VSV-G)-pseudotyped lentivirus was produced in human embryonic kidney (HEK) 293T cells and titrated using NIH-3T3 fibroblasts. The generation of VENUS and VENUS-SDF1α hMSC was performed by plating cells at 6000 cells/cm^2 in 60-mm dishes the day preceding the transduction. HMSC were transduced by overnight incubation with the corresponding lentivirus at a MOI of 20, expanded for up to

four passages and purified by flow cytometry based on their positive expression for the VENUS transgene.

Hypertrophic cartilage engineering

Two million hMSCs were seeded onto type I collagen meshes (cylinder of 6 mm in diameter, 2 mm thick; Ultrafoam, Davol) corresponding to a density of 3.5×10^3 cells/mm^3 to generate hyC. Tissues were cultured for 3 weeks in chondrogenic medium (DMEM supplemented with penicillin-streptomycin glutamine (Invitrogen), HEPES (Invitrogen), sodium pyruvate (Invitrogen), ITS (Insulin, Transferrin, Selenium) (Invitrogen), Human Serum Albumin 0.12% (CSL Behring), 0.1mM ascorbic acid (Sigma), 10^{-7}M dexamethasone (Sigma) and 10ng/ml TGF-β3 (Novartis)), followed by 2 weeks in a serum-free hypertrophic medium (supplemented with 50 nM thyroxine, 7 mM β-glycerophosphate, 10 nM dexamethasone, 0.25 mM ascorbic acid and 50 pg/mL IL-1β) (Scotti et al., 2013).

Gene expression analysis

Total RNA was extracted from cells using TRIzol (Invitrogen, Carlsbad, CA), treated with DNAse and retrotranscribed into cDNA, as previously described (Frank et al., 2002). Real-time RT-PCR was performed with the ABIPrism 77000 Sequence Detection System (Perkin Elmer/Applied Biosystem, Rotkreuz, Switzerland) and expression levels of genes of interest were normalized to GAPDH. Primers and probe sets of osteogenic genes (Collagen type 2, Sox-9, RUNX2, Alkaline phosphatase, Osterix, Bone sialoprotein type 1, SDF1α) were designed and used as previously described (Frank et al., 2002).

Biochemical Stainings

After *in vitro* culture, constructs were fixed in 4% (vol/vol) paraformaldehyde; if necessary, decalcified with 7% (vol/vol) EDTA solution (Sigma); and embedded in paraffin. Sections (5 µm thick) were stained with H&E (Baker) or Alizarin red solution. Histological sections were analyzed using an Olympus BX-61 microscope.

Protein quantification

Protein levels were determined in supernatants collected during *in vitro* chondrogenic differentiation of hyC, and in the final hyC tissue retrieved after 5 weeks of *in vitro* culture.

Samples were analyzed for their content of a panel of growth factors, chemokines, and metalloproteinases, according to the manufacturer's instructions (R&D Immunoassay Kit) and by a Luminex device. Supernatant values were expressed as amounts produced per day per single hyC (pg/mL/day/construct). ECM values correspond to the total content per construct (pg/construct).

Human ossicles generation

In vitro engineered hyC were implanted in subcutaneous pouches of hMCSF / hTPO / hSIRP / -/-Rag2 -/-IL2rg mice, with a maximum of 4 implants per animal. Six weeks after ossicle implantation, 6-8x10^5 cord blood-derived CD34+ cells were pooled from a minimum of 5 donors and injected intravenously into sublethally irradiated immuno-compromised mice (400cGy) as previously reported (Rongvaux et al., 2014, 2011; Scotti et al., 2013). Humanized ossicles were retrieved 6 weeks post-transplantation for subsequent analysis. A minimum of 4 technical experimental replicates was performed. The human cord blood biopsies were approved by the Cantonal ethics committee of Zurich and obtained after informed donor consent.

Mice

Animals consisted in female RAG2−/−γc−/− mice humanized by insertion of human TPO, human M-CSF and human SIRPα. Human TPO and human M-CSF were inserted by knock-in replacement, performed using Velocigene Technology as reported previously (Rongvaux et al., 2011; Willinger et al., 2011). In addition, the Human SIRPα expression was achieved by transgenesis using a BAC in the same genetic background, as previously described (Strowig et al., 2011). All mice were maintained at the University Hospital Zurich animal facility according to the guidelines of the Swiss Federal Veterinary Office, and all the experiments were approved by the Veterinäramt of Kanton Zurich, Zurich, Switzerland (animal permit 187/2013).

Flow cytometry

In vitro samples; cells were retrieved from engineered hyC following digestion using a previously established protocol (Sittinger et al., 2012). Prior to intracellular and nuclear staining, cells were first fixed with fresh formaldehyde 4% and permeabilized by adding ice-

cold 100% methanol slowly to pre-chilled cells, while gently vortexing, to a final concentration of 90% methanol. Cells were then stained for the detection of Sox9 (Abcam), PPARg (Lifesciences), RunX2 (Cell Signaling) and Stro-1 (Biolegend) markers. Analysis were performed on a LSR Fortessa (BD Biosciences).

In vivo samples; Mice were euthanized with CO2 asphyxation and ossicles as well as mouse femur and fibia were removed. Explanted human ossicles and mouse bones were crushed using a mortar and pestle, digested at 37°C for 45 min in DMEM (Invitrogen), 10% FCS (Invitrogen), 10mM HEPES (Invitrogen), 0.4% collagenase II (Worthington) and 0.02% DNase I (Worthington) and washed with PBS containing 2% human Serum and then filtered on a 70 µm cell strainer. The resultant cells were blocked for nonspecific-antibody binding (human and mouse FcR Blocking Reagent, Miltenyi Biotec) and subsequently stained for the markers of interest. All samples were analyzed on a FACS Aria III (BD Biosciences) or LSR Fortessa (BD Biosciences). Antibodies used are listed in **Table S1**.

Colony-forming-unit assay (CFU)

For the colony-forming-unit assays, 1000 hCD45+hlin-hCD34+ cells from ossicle and femur bone marrow were sorted and plated in methylcellulose medium (StemCell Technologies) containing hIL-3 100 ng/ml, hIL-6 50 ng/ml, hIL-11 50 ng/ml, hSCF 50 ng/ml, hTPO 250 ng/ml, hEPO 20 U/ml, hGM-CSF 250 ng/ml and hFlt3L 50 ng/ml. Cultures were maintained at 37°C in 5% CO_2 and scored after 12-14 days.

Micro-computerized tomographic analysis

Microtomography was performed with *in vivo* retrieved ossicles. After fixation in formalin and storage in PBS, microcomputerized tomography data were acquired using a Phoenix nanotom m scanner (General Electric) with 0.5 mm aluminum filtered X-rays (applied voltage, 70 kV; current, 260 µA). Transmission images were acquired during a 360° scan rotation with an incremental rotation step size of 0.25°. Reconstruction was made using a modified Feldkamp algorithm at an isotropic voxel size of 2.5 µm. Threshold-based segmentation and 3D measurement analyses (bone mineral density and volume) were performed using the ImageJ software (ImageJ; National Institutes of Health) with the BoneJ (Meijer et al., 2007) and 3D Shape (Phinney et al., 1999) extensions. 3D rendering of the structures was performed using VGStudio MAX 2.2 software (Volume Graphics).

Immunofluorescence stainings

In vitro or in vivo samples were fixed in 4% (vol/vol) paraformaldehyde; if necessary, decalcified with 7% (vol/vol) EDTA solution (Sigma). Embedding was performed using 4% low-melting agarose (Sigma) and 150 to 250µm thick sections were cut using a Leica VT1200S vibratome with Endurium® low-profile ceramic injector blades (Cadence Inc.). For immunostainings, all steps were performed at room temperature with gentle rocking. Sections were blocked and permeabilized with TBS (final concentration 0.1M Tris, 0.15M NaCl, pH: 7.5) containing 0.05% Tween-20, 20% DMSO (both from Sigma) and 10% donkey serum (Jackson ImmunoResearch). This buffer was also used to dilute all primary antibodies, secondary detection reagents and blocking reagents. After blocking/permeabilization, endogenous avidins and biotins were block using the kit from Vector Labs, each step one hour followed by 30 minutes washes. Sections were then sequentially stained with primary, highly cross-absorbed secondary antibodies and streptavidins (when required), each overnight with 5x1h washes in between using TBS containing 0.05% Tween-20. For staining with two or more primary antibodies raised in the same species, sequential staining was performed with the following blocking steps between: 0.12-0.25mg/mL IgG of the same species as the antibody that needs blocking, 0.12-0.25mg/mL monovalent Fab fragments raised in donkey against the IgG species used in the previous step (both reagents from Jackson ImmunoResearch, both steps overnight), followed if required by additional avidin/biotin blocking steps. A list of primary and secondary antibodies is provided as **Table S2** and **Table S3** respectively.

Optical clearing and mounting of sections

Sections were optically cleared with graded series of 2,2'-thiodiethanol (TDE, Sigma) diluted in TBS until 100% TDE was reached. The final mounting solution consisted of 100% TDE with 0.1M N-propyl gallate (pH: 8.5, Sigma). The refractive index of this solution was measured using a handheld refractometer (Atago) and adjusted to 1.518 with TDE or TBS. Sections were mounted using custom-made silicone spacers (Grace Biolabs) on custom-made size 00, D263M borosilicate coverglass (RI: 1.518, Menzel-Gläser). Sections were mounted on size 1.5 coverslips.

Confocal microscopy

Confocal microscopy was performed on a Leica TCS SP5 equipped with three photomultiplier tubes, two HyD detectors, five lasers (405nm blue diode, argon [458, 476, 488, 496 and 514nm], and three helium neon [543, 594 and 633nm]) using type F immersion liquid (RI: 1.518) and a 20X multiple immersion lens (NA 0.75, FWD 0.680mm). All scans were acquired at 20-25oC, 400Hz, in the bidirectional mode, with z-spacing of 2.49mm (the optical slice thickness of the optics used was 2.69mm). Images were acquired either with a 1.1x to 2.2x optical zoom at a resolution of 512x512 or 1024x1024.

Statistics

Data are presented as means ± standard error of the mean and were analyzed using the GraphPad Prism software. Single comparison was performed using the non-parametric Mann Whitney t-test assuming a non-gaussian distribution of the values. Multiple comparisons were performed using the one-way ANOVA assuming a non-gaussian distribution of the values. Statistical significant differences were defined as: * =$p < 0.05$, ** = $p < 0.01$, *** = $p < 0.001$.

References

Frank, O., Heim, M., Jakob, M., Barbero, A., Schafer, D., Bendik, I., Dick, W., Heberer, M., Martin, I., 2002. Real-time quantitative RT-PCR analysis of human bone marrow stromal cells during osteogenic differentiation in vitro. J Cell Biochem 85, 737–746. https://doi.org/10.1002/jcb.10174

Meijer, G.J., De Bruijn, J.D., Koole, R., Van Blitterswijk, C.A., 2007. Cell-based bone tissue engineering. PLoS Med. 4, 0260–0264. https://doi.org/10.1371/journal.pmed.0040009

Phinney, D.G., Kopen, G., Righter, W., Webster, S., Tremain, N., Prockop, D.J., 1999. Donor variation in the growth properties and osteogenic potential of human marrow stromal cells. J. Cell. Biochem. 75, 424–36. https://doi.org/10.1002/(SICI)1097-4644(19991201)75:3<424::AID-JCB8>3.0.CO;2-8

Rongvaux, A., Willinger, T., Martinek, J., Strowig, T., Gearty, S. V, Teichmann, L.L., Saito, Y., Marches, F., Halene, S., Palucka, A.K., Manz, M.G., Flavell, R.A., 2014. Development and function of human innate immune cells in a humanized mouse model. Nat Biotechnol 32, 364–372. https://doi.org/10.1038/nbt.2858

Rongvaux, A., Willinger, T., Takizawa, H., Rathinam, C., Auerbach, W., Murphy, A.J., Valenzuela, D.M., Yancopoulos, G.D., Eynon, E.E., Stevens, S., Manz, M.G., Flavell, R.A., 2011. Human thrombopoietin knockin mice efficiently support human hematopoiesis in vivo. Proc. Natl. Acad. Sci. U. S. A. 108, 2378–83. https://doi.org/10.1073/pnas.1019524108

Schambach, A., Galla, M., Modlich, U., Will, E., Chandra, S., Reeves, L., Colbert, M., Williams, D.A., von Kalle, C., Baum, C., 2006. Lentiviral vectors pseudotyped with murine ecotropic envelope: Increased biosafety and convenience in preclinical research. Exp. Hematol. 34, 588–592. https://doi.org/10.1016/j.exphem.2006.02.005

Scotti, C., Piccinini, E., Takizawa, H., Todorov, A., Bourgine, P., Papadimitropoulos, A., Barbero, A., Manz, M.G., Martin, I., 2013. Engineering of a functional bone organ through endochondral ossification. Proc. Natl. Acad. Sci. U. S. A. 110, 3997–4002. https://doi.org/10.1073/pnas.1220108110

Sittinger, M., Hamouda, H., Ringe, J., Stich, S., Ullah, M., 2012. A Reliable Protocol for the Isolation of Viable, Chondrogenically Differentiated Human Mesenchymal Stem Cells from High-Density Pellet Cultures. Biores. Open Access. https://doi.org/10.1089/biores.2012.0279

Strowig, T., Rongvaux, A., Rathinam, C., Takizawa, H., Borsotti, C., Philbrick, W., Eynon, E.E.,

Manz, M.G., Flavell, R. a, 2011. Transgenic expression of human signal regulatory protein alpha in Rag2-/-gamma(c)-/- mice improves engraftment of human hematopoietic cells in humanized mice. Proc. Natl. Acad. Sci. U. S. A. 108, 13218–23. https://doi.org/10.1073/pnas.1109769108

Willinger, T., Rongvaux, A., Takizawa, H., Yancopoulos, G.D., Valenzuela, D.M., Murphy, A.J., Auerbach, W., Eynon, E.E., Stevens, S., Manz, M.G., Flavell, R.A., 2011. Human IL-3/GM-CSF knock-in mice support human alveolar macrophage development and human immune responses in the lung. Proc Natl Acad Sci U S A 108, 2390–2395. https://doi.org/10.1073/pnas.1019682108

Supplementary Materials

Antibody	**Conjugated fluorophore**	**Specie**	**Company**	**Product number**
human lineage cocktail	PE Cy5	Mouse	Invitrogen	348807
human CD45	eFluor 450	Mouse	eBioscience	48-0459-42
human CD90	PE	Mouse	BD	555596
Human CD38-biotin	Streptatividin-Pacific orange	Mouse	Biolegend	303518
human CD34	PECy7	Mouse	BD	348811
human CD45RA	APC eFluor 780	Mouse	eBioscience	47-0458-42
mouse CD45	APC	Mouse	Biolegend	109814

Table 1. List of antibodies used for flow cytometry analysis, Related to Figure 3.

Primary antibody	Specie	Company	Product number
Collagen type 2	Mouse	Abbiotec	250484
SDF1α	Rabbit	eBiosciences	14-7992-81
Laminin	Rabbit	Novus BIologicals	NB300-144
Peripherin	Rabbit	Biolegend/Covance	PRB-576C
Alkaline Phosphatase	Goat	R&D systems	AF2910
CD34	Rabbit	Novus Biologicals	NBP2-38322
CD90	Sheep	R&D systems	AF2067
human CD45	Rat	AbD Serotec	MCA345GT
GFP	Chicken	Aveslab	GFP-1020

Table 2. List of primary antibodies used for confocal immunofluorescence analysis, Related to Figure 4.

Secondary antibody	Specie	Company	Product number
Anti-rat Alexa Fluor 488	Donkey	Thermofischer	A-21208
Anti-rabbit Alexa Fluor 555	Donkey	Thermofischer	A-31572
Anti-mouse Alexa Fluor 555	Donkey	Thermofischer	A-31570
Anti-rat	Donkey	Thermofischer	A-21096

Alexa Fluor 680			
Anti-rat CF633	Donkey	Biotium	20137
Anti-goat Alexa fluor 594	Donkey	Thermofischer	A-11058
Anti-rabbit CF633	Donkey	Biotium	20125
Anti-chicken	Donkey	Jackson Immunoresearch	703-545-155

Table 3. List of secondary antibodies used for confocal immunofluorescence analysis, Related to Figure 4.

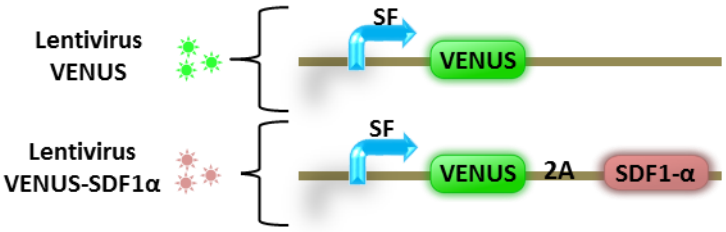

Figure S1. Lentivectors overview used for the generation of VENUS and VENUS-SDF1α hMSCs populations, Related to Figure 1.

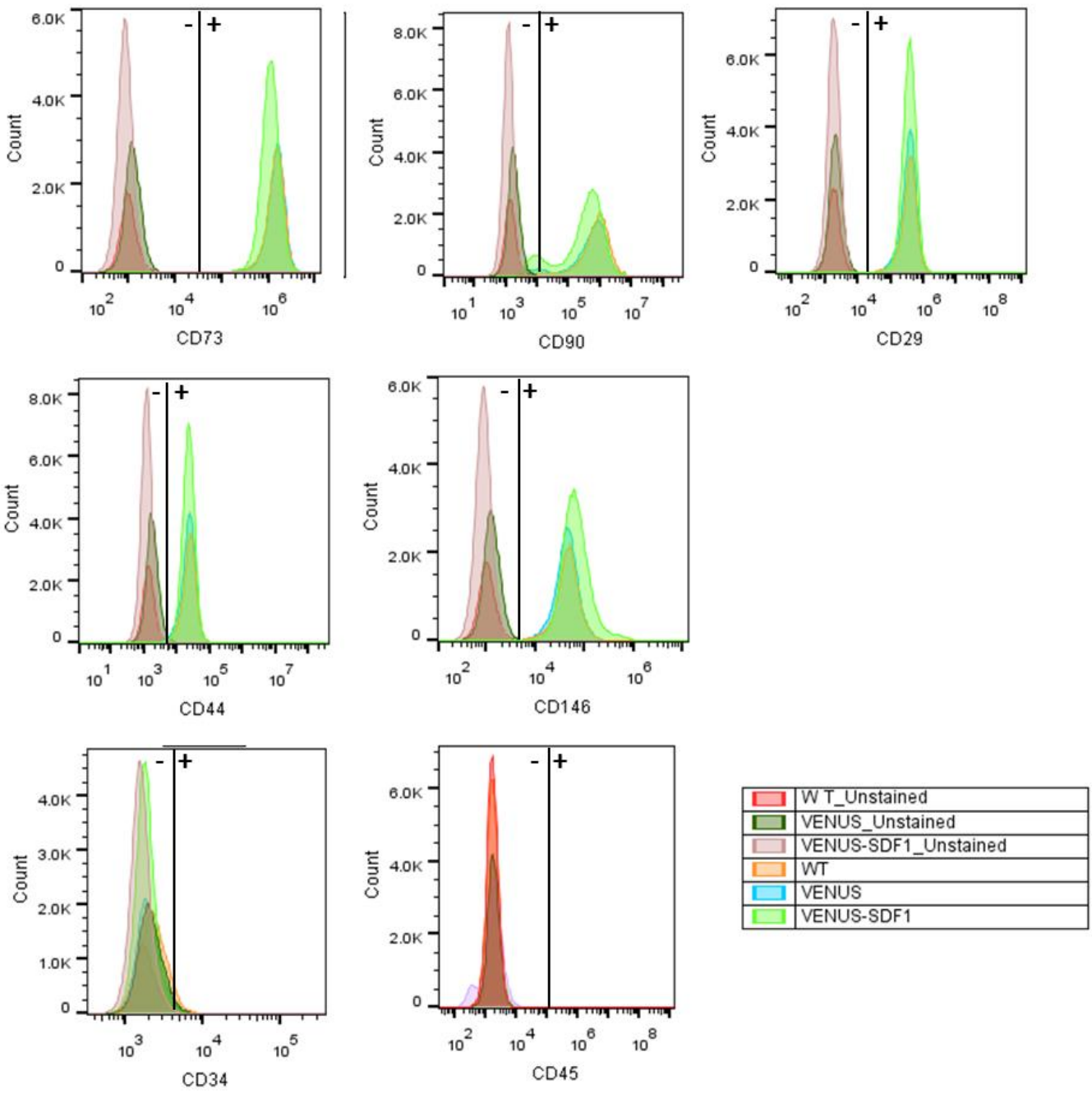

Figure S2. Comparable phenotypes of hMSCs untransduced (WT = primary hMSCs) and transduced with the VENUS or VENUS-SDF1α lentiviruses. All cells express CD73, CD90, CD29, CD44, CD146 but not CD34 and CD45. Data compiled from flow cytometry analysis, Related to Figure 1.

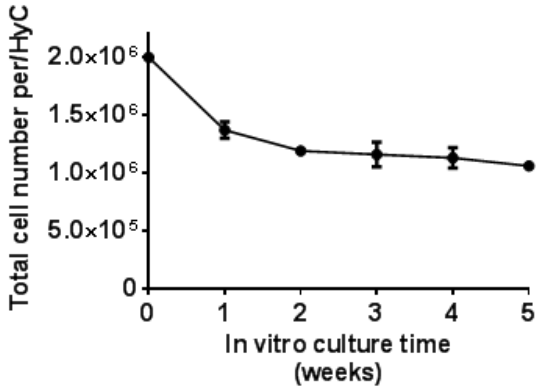

Figure S3. Quantification by DNA content of hMSC number in hyC over in vitro culture time, Related to Figure 1. n=3 biological replicates.

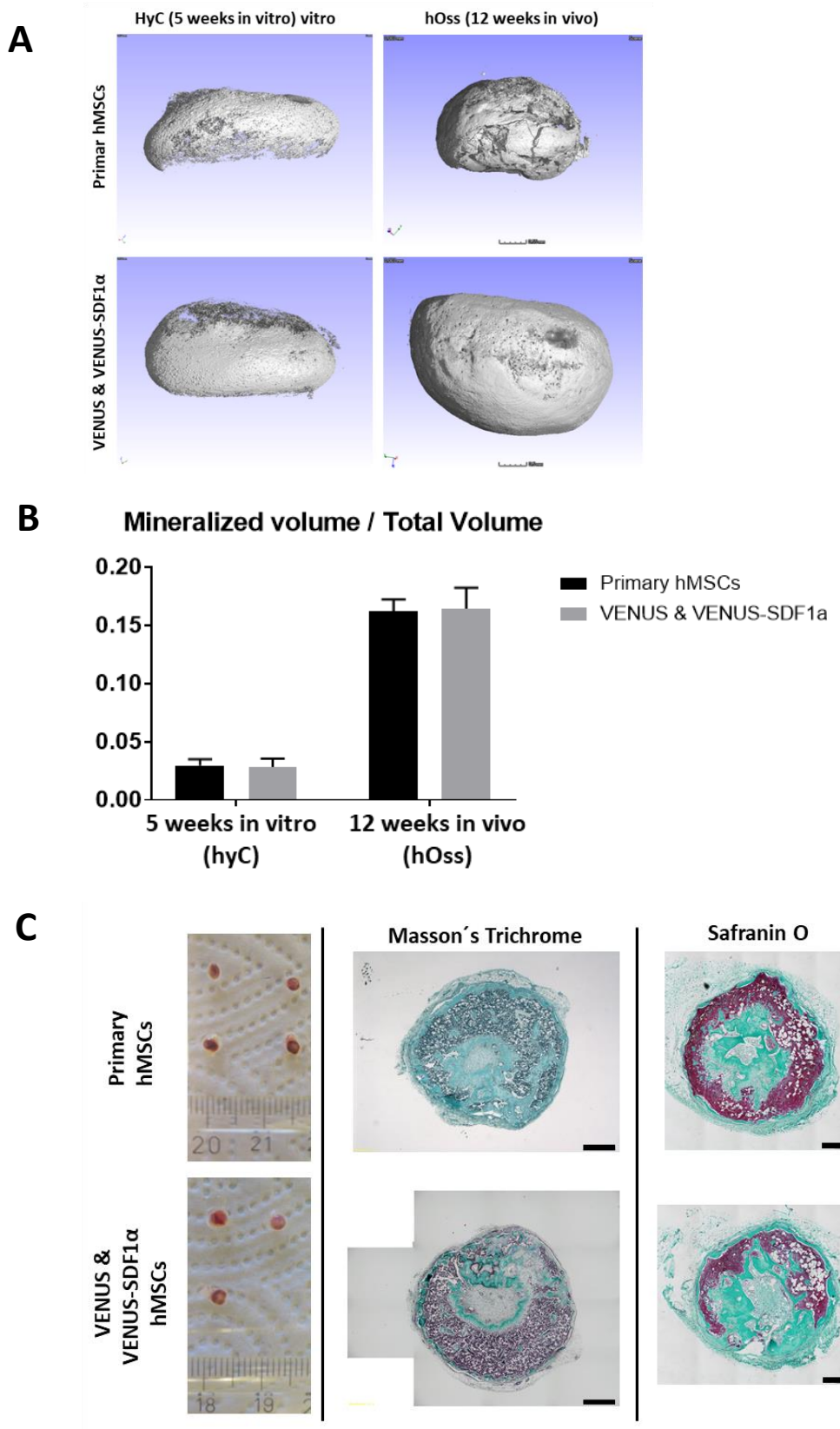

Figure S4. Histological and microcomputed analysis of engineered tissues, Related to Figure 3. (A) Representative MicroCT reconstitution of hyC and hOss generated from untransduced (primary hMSCs) or transduced hMSCs (VENUS & VENUS-SDF1α). (B) Quantification of the

mineral volume in the respective hyC and hOss. Data were then normalized to the average volume of the respective tissues, to display the final mineralized volume over total volume. n≥3. (C) Histological analysis of hOss generated from primary or transduced hMSCs (VENUS and VENUS-SDF1α). No differences could be observed between the two groups. hOss were explanted 12 weeks post-in vivo implantation. Scale bar = 500µm.

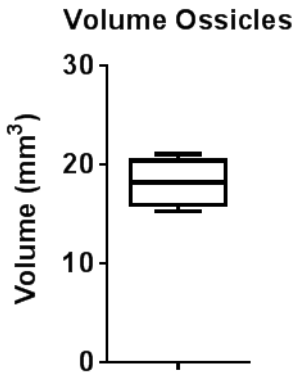

Figure S5. Mean volume of hOss (18 ±2.1 mm3) calculated by microtomography, Related to Figure 3. n=6 biological replicates. Data are represented as mean +/- SEM.

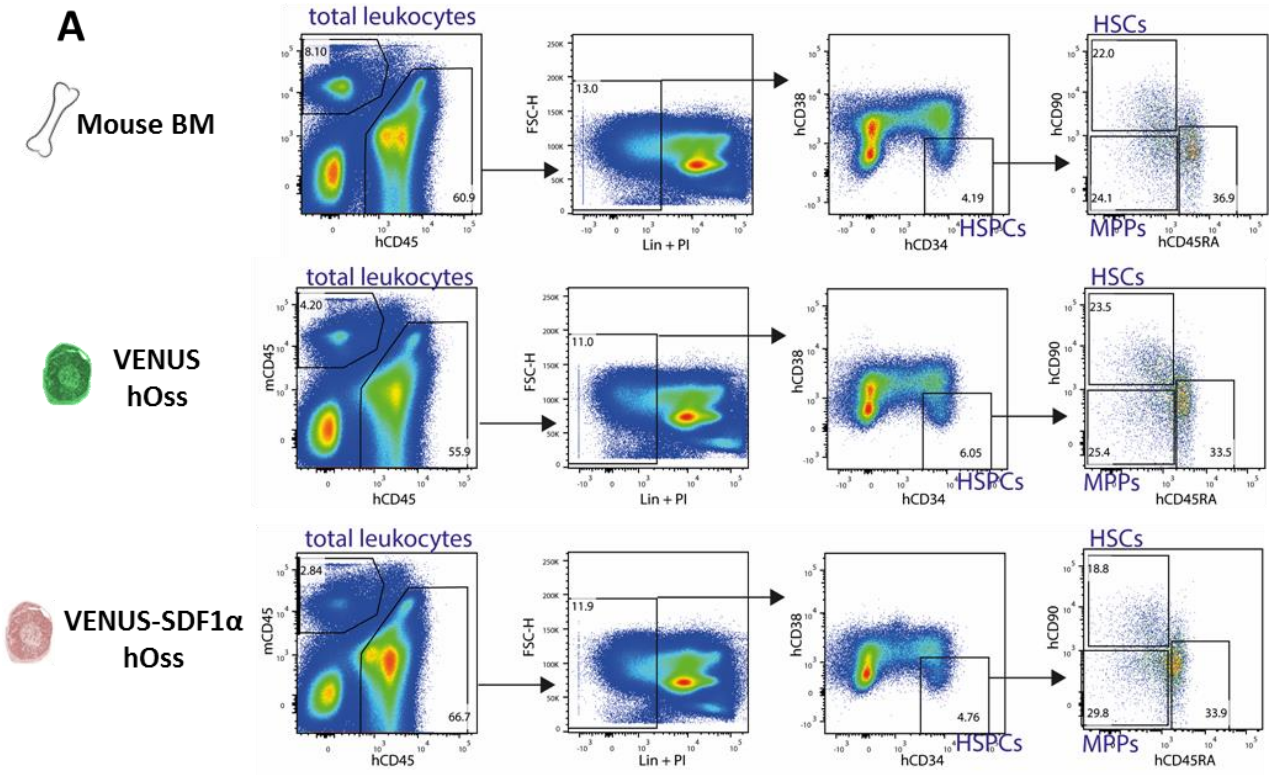

B

Population	Surface phenotype
HSPCs	Lin- CD34+ 38-
HSCs	Lin- hCD45+ CD34+ CD38- CD45RA- CD90+
MPPs	Lin- hCD45+ CD34+ CD38- CD45RA- CD90-
MylPs	Lin- hCD45+ CD34+ CD38- CD45RA+ CD90-
CMPs/MEPs	Lin- hCD45+ CD34+ CD38+ CD45RA-
GMPs	Lin- hCD45+ CD34+ CD38+ CD45RA+

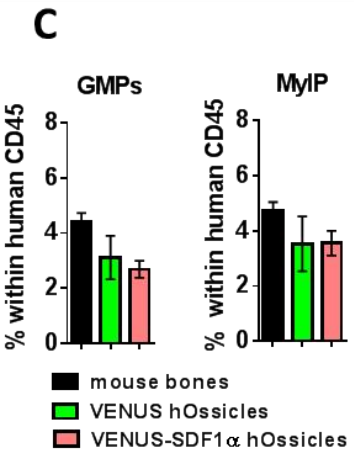

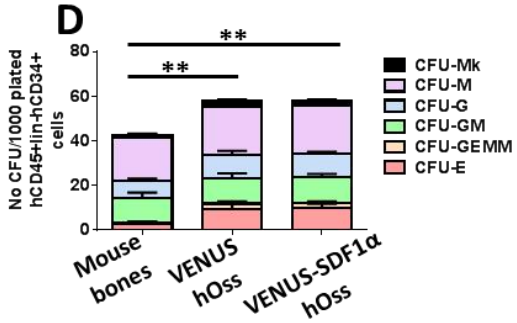

Figure S6. Bone marrow analysis of mouse bones and human ossicles, Related to Figure 3. (A) Gating strategy for analysis of HSPCs populations engrafted in mouse bones or humanized ossicles. (B) Phenotypic markers defining HSPCs, HSCs, MPPs, Myeloid progenitors (MylPs),

CMPs/MEPs and Granulocyte-monocyte progenitors (GMPs) populations. (C) Flow cytometry-derived frequencies of GMP amd MyLP populations in engineered hOss and mouse bones at the end of the 12 weeks *in vivo* period. n ≥12. (D) Human CD45+/CD34+ cells maintained in VENUS and VENUS-SDF1α ossicles displayed a superior capacity to form myeloid colonies *in vitro*. CFU: colony forming unit. GEmM: Colony-forming unit-Granulocyte, Erythroid, macrophage, Megakaryocyte. GM: Colony-forming unit-granulocyte and macrophage. E: colony forming unit-erythroid. G: colony forming unit granulocyte. M: colony forming unit macrophage. n ≥12 biological replicates. *p<0.05, **p<0.01. Data are represented as mean +/- SEM.

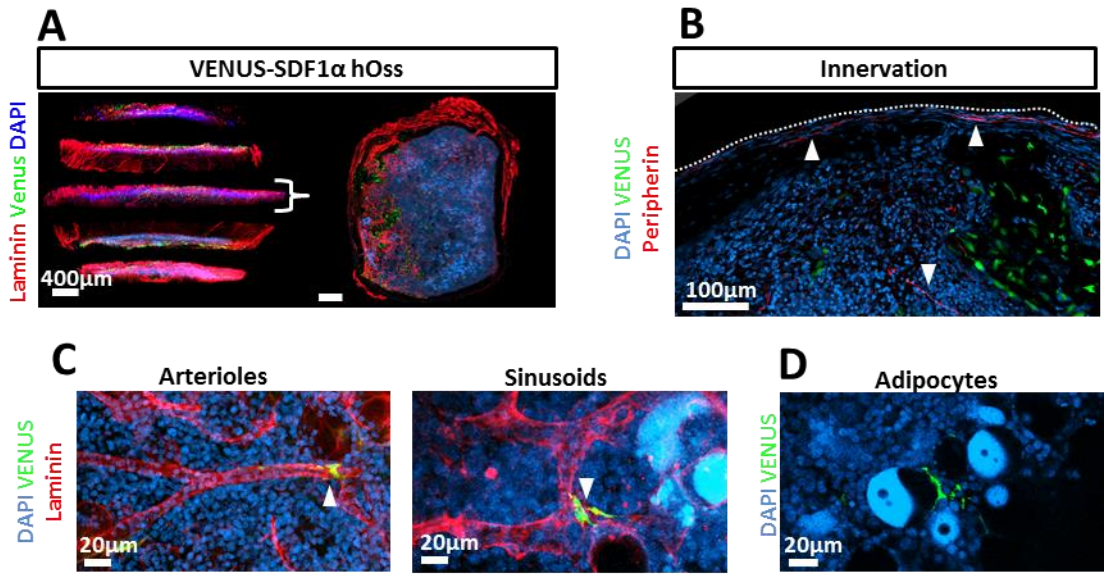

Figure S7. Confocal analysis of VENUS-SDF1α ossicles, Related to Figure 4. (A) Multidimensional confocal immunofluorescence imaging of VENUS-SDF1αhOss for 3D quantitative information retrieval (left). Top view of a transversal hOss section (right) illustrating the internal bone marrow cavity (DAPI) and intense peripheric vascularization (lamimin). Scale bar = 400µm. (B) Humanized ossicles display evidences of innervation (arrows), proving connection to the host nervous system. Dashline indicates the external border of the hOss. Scale bar = 100µm. (C) Implanted hMSC (VENUS positive) are detected in association with the established vasculature, which includes both arterioles (left) and sinusoids (right). Scale bar = 20µm. (D) Implanted hMSCs (VENUS positive) differentiate into adipocytes, as assessed by the presence of cytosolic lipid droplets autofluorescent in the blue channel (DAPI). Scale bar = 20µm.

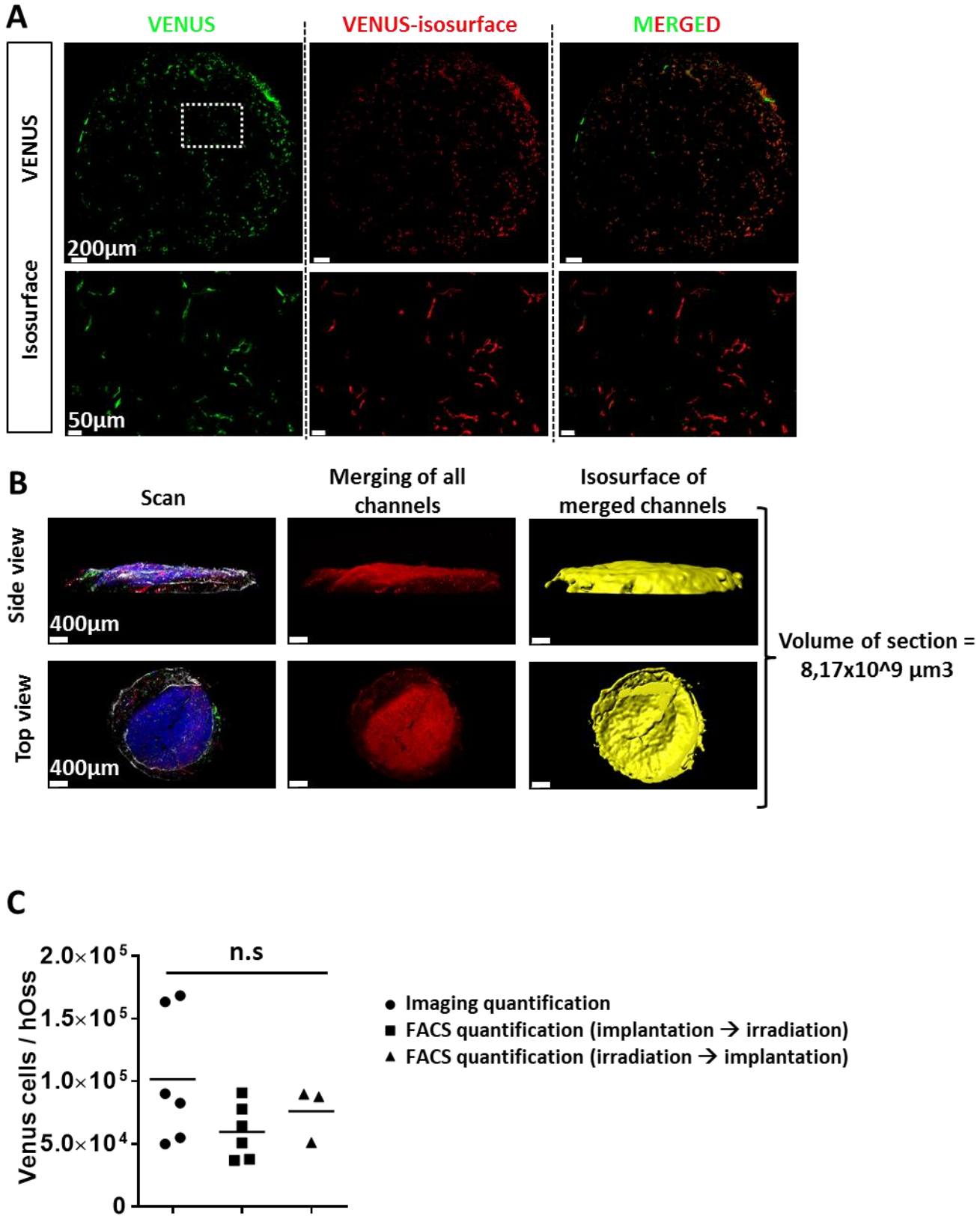

Figure S8. Imaging strategy for hMSCs quantification in humanized ossicles, Related to Figure 4. (A) Generation of isosurfaces for hMSC-VENUS fate determination/quantification using the

Imaris software. (B) Generation of isosurfaces of whole sections based on the combination of all channels using the Imaris software. This is used to derive the volume of section scanned and normalized the number of objects per volume of section. (C) Quantification of VENUS expressing hMSCs by segmentation of confocal scans and by flow cytometry based on the VENUS signal following digestion of hOss. One point represents one ossicle, the bar represents the mean. Significance was assessed by one-way ANOVA test.

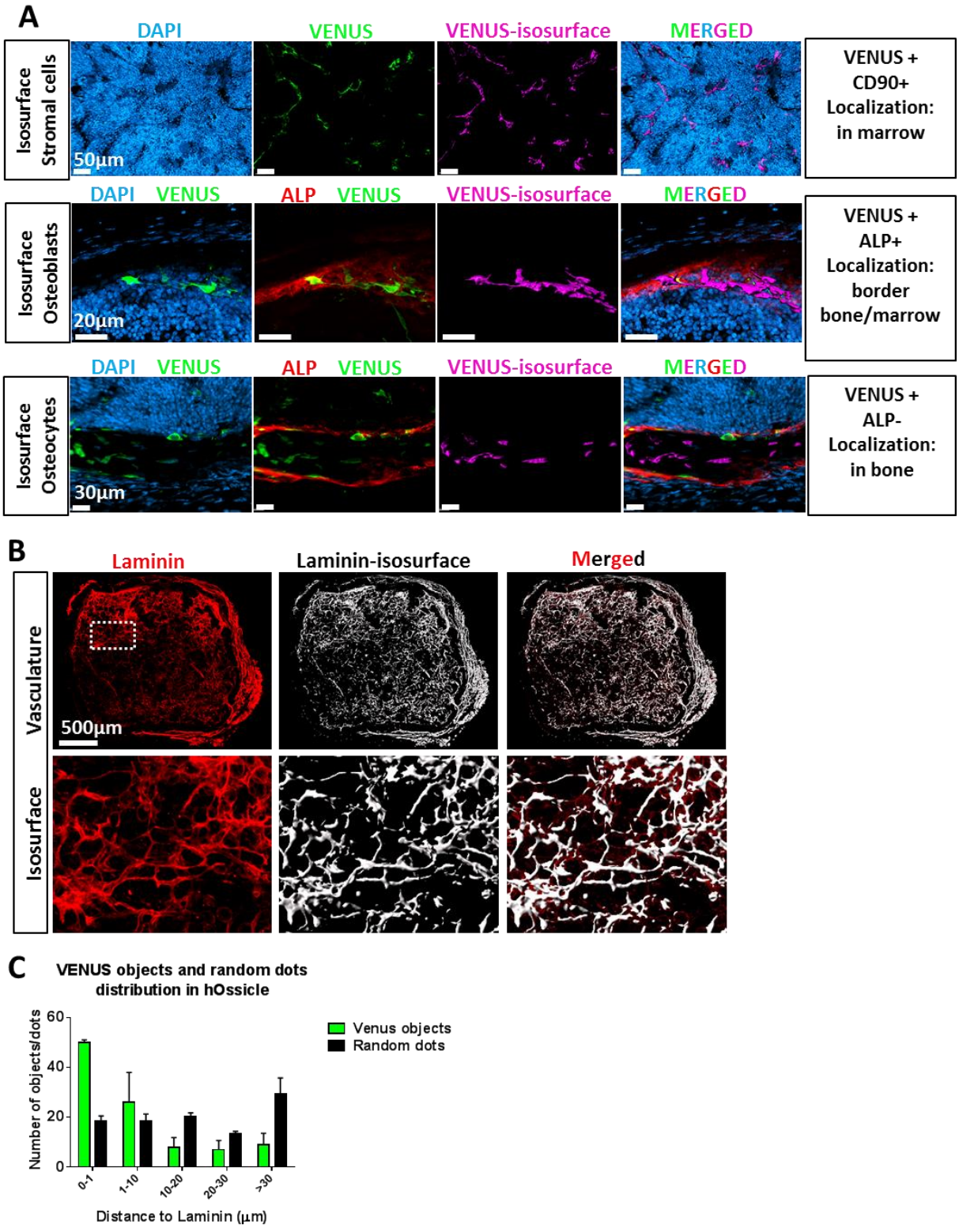

Figure S9. Isosurface strategies for the quantification of hMSCs fate in humanized ossicles, Related to Figure 4. (A) Rationale and representative example leading to the generation of isosurfaces for hMSC-VENUS fate determination/quantification. ALP: alkalyne phosphatase. (B) Generation of vasculature isosurfaces using laminin expression as a proxy for vasculature.

(C) Distance transform between VENUS objects and Laminin, and comparison with random dots distribution. Data are represented as mean +/- SEM.

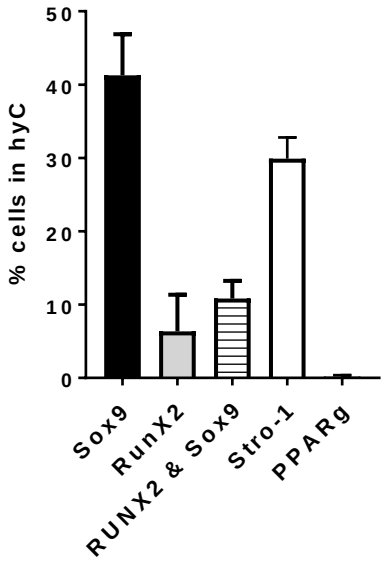

Figure S10. Intracellular staining of hMSCs retrieved from engineered hyC (5 weeks of *in vitro* differentiation), Related to Figure 4. Stainings for the transcription factors Sry-box 9 (Sox-9), Runt-related transcription factor 2 (RunX2), peroxisome proliferator-activated receptor gamma (PPARg) and Stro-1 were used as chondrocytic, osteoblastic, adipocytic or progenitor marker, respectively. Most of the hMSCs display lineage commitment, but some maintain the expression of the Stro-1 progenitor marker. n=2 independent experiments, N≥6 biological replicates. Data are represented as mean +/- SEM.

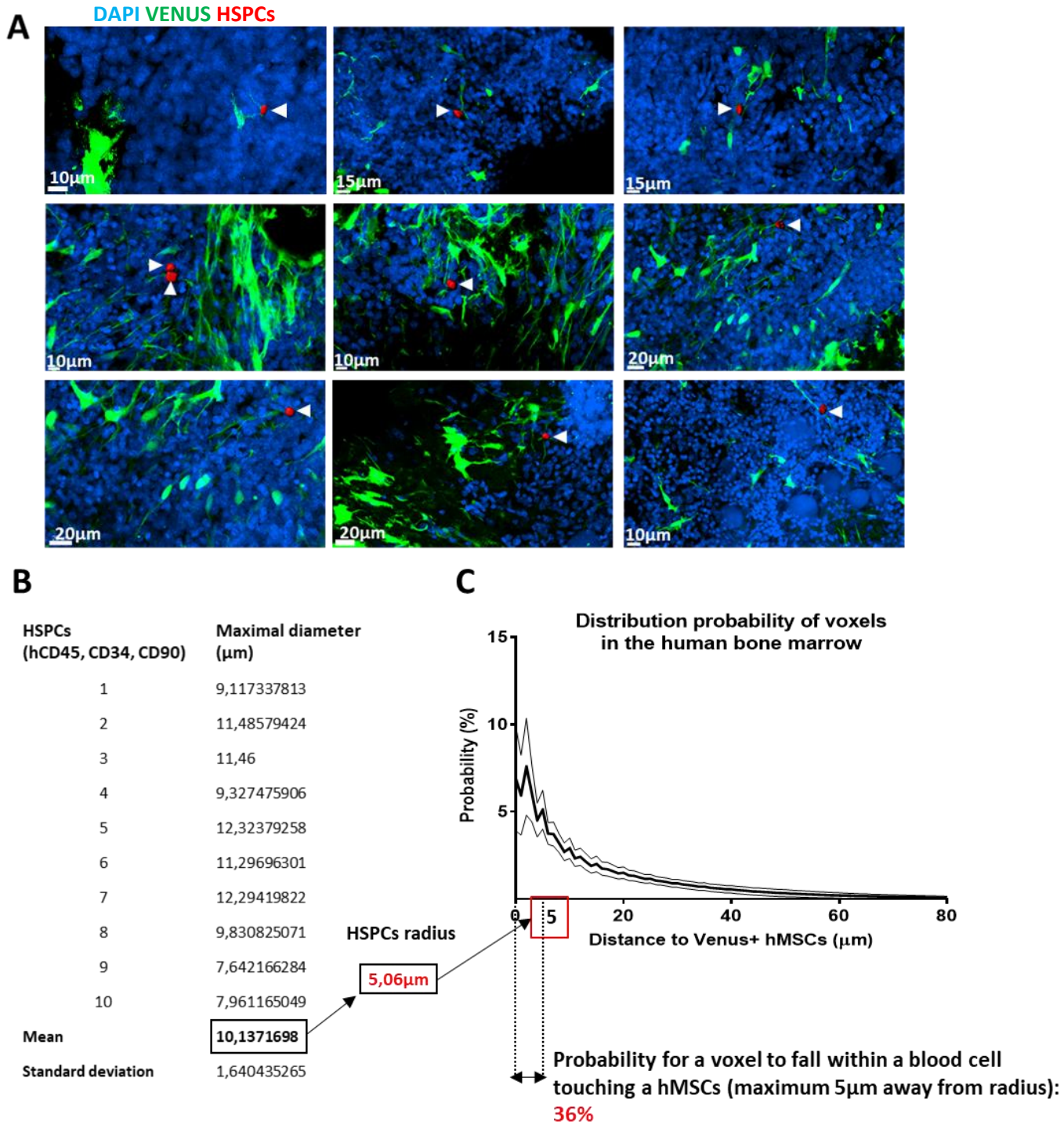

Figure S11. Probability assessment of voxels to randomly distribute in a HSPCs touching a hMSCs, Related to Figure 4. (A) Confocal images of detected HSPCs (red objects defined by hCD45+/CD34+/CD90+) touching hMSCs (VENUS). (B) Maximal diameter calculation of HSPCs (n=10) allowed to determine the HSPCs radius (5µm). Any blood cells in physical contact with a hMSC will thus have its center maximum 5µm away from this hMSC. (C) Distance probability between randomly distributed voxels and hMSCs within the human bone marrow volume.

This was calculated by distance transform using the segmented isosurface of hMSCs (VENUS signal) and of the human hematopoietic compartment (based on the human CD45 signal). The central line (thick pattern) represent the mean. The upper and lower lines represent the mean of maximal and minimal values respectively. All voxels falling within a 0 to 5µm distance (corresponding to the maximum HSPCs radius) would thus necessary be confined in a blood cells touching a hMSC. Thus, the probability that a voxel falls directly within a blood cell in physical contact with hMSCs is of 36%. Data were compiled out of n=4 confocal scans.